On the Effect of Leading Edge Serrations on Aerofoil Noise Production

Tze Pei Chong[1], Till Biedermann[2], Oliver Koster[3] and Seyed Mohammad Hasheminejad[4]

[1, 4] *Brunel University London, Uxbridge, UB8 3PH, United Kingdom*
[2, 3] *University of Applied Sciences Dusseldorf, Dusseldorf 40474, Germany*

This paper presents experimental results on the aeroacoustic performances of a NACA 65(12)-10 aerofoil subjected to serrated leading edges. The serration patterns of these leading edges are formed by cutting into the main body of the aerofoil, instead of extending the leading edges. Therefore these serrated leading edges, when attached to the main body of the aerofoil, will always result in the same overall chord length. The experiment was performed in an aeroacoustic wind tunnel facility. These serrated leading edges were investigated for their effectiveness in suppressing four different types of noise sources: laminar instability tonal noise, leading edge separation bubble noise, turbulence–leading edge interaction noise and trailing edge self-noise. Streamwise vortices produced by an optimised serrated leading edge can suppress the separation bubble at the trailing edge, thereby reducing the instability laminar tonal noise significantly. It is found that the most effective serration configuration is the one with the largest serration amplitude and smallest serration wavelength. Without even relying on the streamwise vortices, the sawtooth geometry of the serration itself can already be sufficient to suppress the leading edge separation bubble. Due to the special geometry of the NACA 65(12)-10, it is very effective in the production of laminar separation bubble noise at the leading edge. The use of serrated leading edge can therefore be an effective passive device to suppress this particular noise source. Similarly, the most effective serration geometry in the reduction of turbulence–leading edge interaction noise is the one with the largest serration amplitude and smallest serration wavelength. However, this configuration is also prone to generating superfluous noise at high frequency. Extensive boundary layer and very near wake measurements were performed to investigate the flow structures on the NACA 65(12)-10 aerofoil with a large serration amplitude leading edge. It can be concluded that the serrated leading edge is very disruptive to the hydrodynamic growth of the turbulent boundary layer at the trailing edge. Evidences on the reduction of boundary layer low-frequency turbulence at the trailing edge could support the hypothesis of a reduction in the low-frequency far field noise. This remains to be confirmed in the future studies.

[1] Senior Lecturer, Department of Mechanical and Aerospace Engineering, t.p.chong@brunel.ac.uk, AIAA Member
[2] PhD student, Institute of Sound and Vibration Engineering ISAVE, till.biedermann@hs-duesseldorf.de AIAA student member.
[3] Master student, Institute of Sound and Vibration Engineering ISAVE, oliver.koster@study.hs-duesseldorf.de Non-AIAA member.
[4] Postdoctoral research fellow, Department of Mechanical and Aerospace Engineering, m.hasheminejad@brunel.ac.uk. Non-AIAA member.

I. Introduction

Energy harvested from wind turbine is clean, and represents an alternative for fossil energy. However, when the wind turbine blades move through the air, significant level of aerodynamic noise is generated. To protect residents, maximum noise levels are set that may not be exceeded. To stay within the noise limit, wind turbines often need to operate at reduced speed, which causes the wind energy effectively more expensive to generate. Reduction of blade noise without reducing the rotor speed would therefore make wind energy cheaper. This point was re-iterated during a scientific workshop recently held at the Lorentz Center at Leiden, Netherland on "Serration Technology on Airfoil: Unsteady Aerodynamic and Aeroacoustics" 17–21 Oct 2016. In particular, a further 1 dB noise reduction above the current level can lead to significant increase in wind energy production (i.e. the turbine blades can operate in longer hours and at a faster rotating speed). Therefore wind turbine manufacturers are actively seeking new technology to further reduce the level of aerodynamic noise of their turbine blades.

Wind turbine noise can be generated at the trailing edge where turbulence in the boundary layer that develops on the blade surface scatters into sound (i.e. self-noise). The most effective approach to reduce the wind turbine trailing edge noise thus far is the application of owl wing-inspired serrated sawtooth trailing edges. They are so versatile that significant self-noise reduction can be achieved regardless whether the serration is formed either by the cut-in approach[1-3], or the add-on approach [4-6].

Through interaction with the atmospheric turbulence, the leading edge of a wind turbine blade can also be an effective noise source. It has been shown in the previous studies that leading edge noise is normally related to the convective large-scale turbulence structures in the freestream. These turbulence structures interact with the leading edge of an aerofoil before being stretched around it, and in the process, induce large pressure fluctuations on the suction and pressure sides of the aerofoil. Significant level of broadband noise radiation is produced as a result of the amplified unsteady lift [NOISE SOURCE A]. To reduce the leading edge noise, one of the most effective methods, again, is to apply the owl-inspired serrated pattern at the leading edge. Some studies performed on owl's silent flight (mainly through measurements of mid-flight noise emissions) have led to postulations that these serrations could be partially responsible for the unique in-flight noise reduction capability of an owl. Many experimental[7-9] and numerical[10, 11] studies have now proven that forming a serrated pattern at the aerofoil leading edge can lead to significant turbulence interaction noise reduction.

Another possible aerofoil noise radiation near the leading edge, which is relatively less studied, originates from the local separation bubble [NOISE SOURCE B]. Through the use of NACA 65(12)-10, Lacagnina et al.[12] identified that the low-frequency hump with a central frequency of $fC/U \approx 15$ in their acoustic spectra is related to the separation bubble at the pressure side leading edge at zero or negative angles of attack. Here f is the frequency, C is the aerofoil chord and U is the freestream velocity. These low-frequency humps disappear as soon as leading edge serration is introduced. They claimed that the large-scale turbulence structures near the trailing edge that are otherwise present in the baseline case will be suppressed when serrated leading edge is used. This suggests that the reduction of the low-frequency hump could be related to the trailing edge self-noise. On the other hand, direct noise radiation by the separation bubble could also be a possibility. Since the origin of the low-frequency hump remains unconfirmed, it is necessary to also pay attention to the local flow effects of the separation bubble and its role in the noise radiation.

When the incoming mean flow interacts with the serrated leading edge aerofoil, vortical structures with large streamwise vorticity may be generated (mostly from the troughs) as a by-product. If the amplitude (tip-to-trough distance) of the serrated leading edge is sufficiently large, these secondary flows could be amplified sufficiently to overcome the viscous dissipation by the boundary layer and disturb the hydrodynamics at the aerofoil trailing edge. In this scenario, it is hypothesised that injection of streamwise vorticity into the boundary layer near the trailing edge could indeed affect the self-noise radiation, which is in line with the conjecture made by Lacagnina et al.[12]. Depends on the level of freestream turbulence intensity, Reynolds number, angles of attack for the aerofoil and aerofoil type, boundary layer near the trailing edge could either be laminar or turbulent, which would produce instability tonal noise (NOISE SOURCE C) and broadband noise (NOISE SOURCE D), respectively. These two noise sources have very different acoustic characteristics and generation mechanisms.

This paper will investigate the effect of serrated leading edges on the four noise sources described above, individually, through surface flow visualisation, boundary layer and near wake measurements. These hydrodynamic data will be compared against the acoustic data which were measured at the same aeroacoustic facility and flow condition. For noise sources B and C, low-freestream turbulence intensity is a pre-requisite. To study the effect of serrated leading edge on the noise source A, turbulence-grid is used to generate elevated-level of freestream turbulence intensity. Noise source D also plays a prominent role in the aerofoil noise production. In order to generate a turbulent boundary layer at the trailing edge experimentally, trip tape is usually used to trip the upstream

boundary layer into an instantaneous bypass transition. However, in the current study where serrated leading edge is used, the presence of trip tape downstream the serration might affect the natural growth of the secondary flow emanated from the sawtooth troughs. Instead, investigation of the effect of serrated leading edge on noise source D is performed at the same flow condition as that for the noise source A, i.e. no boundary layer trip tape is used. Instead we rely on the elevated freestream turbulence intensity which has been confirmed to trigger a bypass-transition in the boundary layer on both sides of the aerofoil surface.

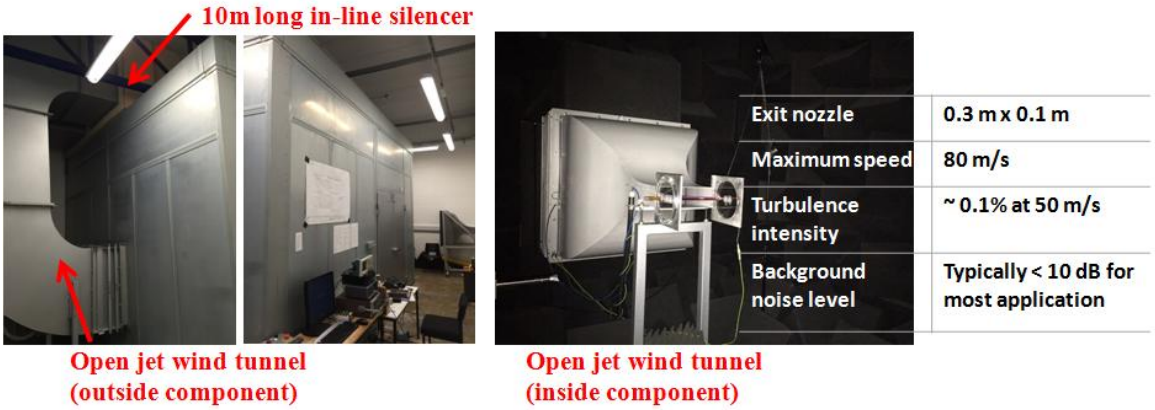

Fig. 1 Aeroacoustic wind tunnel and anechoic chamber

II. Experimental setup

A. Wind tunnel facilities and instrumentations

Free field measurements of the aerofoil noise were conducted in the aeroacoustic wind tunnel at Brunel University London, which is situated in a 4 m x 5 m x 3.4 m anechoic chamber. As shown in Fig. 1, the nozzle exit is rectangular with dimensions of 0.10 m (height) x 0.30 m (width). This wind tunnel can achieve a turbulence intensity of between 0.1–0.2% (thus it is suitable for the study of noise sources B and C). The background noise of the wind tunnel facility is well below the self-noise of the quietest aerofoil across the whole range of velocity[13]. The range of jet speeds under investigation was between 20 ms^{-1} and 60 ms^{-1}, corresponding to Reynolds numbers based on aerofoil chord, C of 2×10^5 and 6×10^5 respectively. The aerofoil was held by side plates and attached flushed to the nozzle lips. It should be noted that the aerofoil is always positioned at zero degree angle of attack with relative to the main jet direction throughout the investigation of the four noise sources. Far field noise measurements were made by a single condenser microphone at a distance of 1.0 m from the aerofoil mid-span. Noise data from the microphone was acquired at a sampling frequency of 44 kHz for 10 seconds by a 16-bit Analogue-Digital card from National Instrument. The data was then windowed and the Power Spectral Density (PSD) of 1 Hz bandwidth computed from a 1024 point fast Fourier transform.

Oil flow visualisation was conducted on the suction side of the aerofoil surface to examine the dynamic changes of near wall properties subjected to the serrated leading edges. It is also performed at the pressure side of a straight leading edge aerofoil in another study. The oil mixture used in this study consists of three components: linseed oil providing the oil base of the compound, titanium dioxide as a colouring agent, and paraffin for controlling the viscosity of the compound. Care was taken to obtain an appropriate viscosity of the compound. It should be noted that application of the oil compound to the aerofoil surface is unlikely to affect the boundary layer significantly, especially when observing the large scale vortex formation from the serrated leading edges.

Single boundary layer type hot wire probe (5μm diameter DANTEC 55P15) was used to measure the mean and fluctuating velocities of the aerofoil boundary layer at an overheat ratio of 1.8. Signals from the hot wire were digitised by a 12-bit A/D converter at a sampling frequency of 20 kHz for 13.1 seconds (256,000 samples). For the wake measurement, an X-wire probe (DANTEC 55P61) was used to measure two velocity components simultaneously. The overheat ratio for both wires were set at a slightly lower value of 1.6 in order to avoid thermal interference between them at low speed. Both the velocity and yaw calibrations of the X-wire were done in-situ. The same sampling frequency and sampling time as the single wire boundary layer probe was employed for the X-wire.

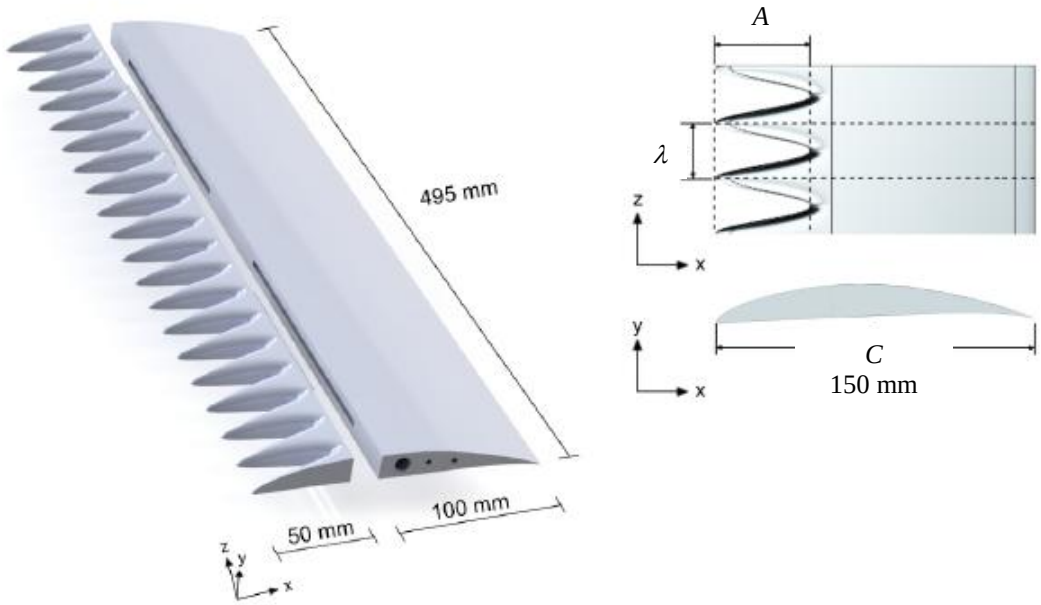

Fig. 2 NACA 65(12)-10 model. Left: Isometric drawing with the detachable serrated leading edge (λ26A45) and main body, Right: Top and side views of aerofoil including some geometrical parameters.

B. Aerofoil model and the serrated leading edge designs

As shown in Fig. 2, the aerofoil under investigation here is a NACA 65(12)-10, cambered aerofoil. The chord length, C is 150 mm, and the width is 495 mm. Note that, during the aeroacoustic measurement, only 300 mm width is submerged inside the jet flow. The remaining width is extended outside the side plate. The reason to have a wider aerofoil than needed for the aeroacoustic test is that the same aerofoil will be used in another wind tunnel for aerodynamic force measurement, which is not the main focus for the current paper. The serrated leading edges were cut directly into the main body of the aerofoil. This will preserve the aerofoil chord length, but reduce the overall wetted area of the aerofoil. Between the leading edge $x/C = 0$, and $x/C = 0.33$, is a section that can be removed and replaced by different serration profiles. Note that x is the streamwise direction. Further downstream, $0.33 < x/C \leq 1.0$, is the unmodified aerofoil main body. Once the serrated leading edge is attached to the main body a continuous profile is formed giving the appearance that the serrated patterns are cut into the main body of the aerofoil. A total 12 serrated leading edge sections, plus one with straight leading edge to serve as a baseline case, were investigated in this study.

When describing the serration pattern, two geometrical parameters are normally defined, which are shown in Fig. 2 as the wavelength, λ and the amplitude, A. Note that the naming of each serrated leading edge, including the baseline case, is in accordance to the values of their serration wavelength λ, and serration amplitude A. For example, the "clean", baseline leading edge, which does not contain any serration wavelength and serration amplitude, is therefore named as $\lambda 0A0$. Likewise, the serrated leading edge that has a serration wavelength of 7.5 mm and serration amplitude of 45 mm will be named as $\lambda 7.5A45$.

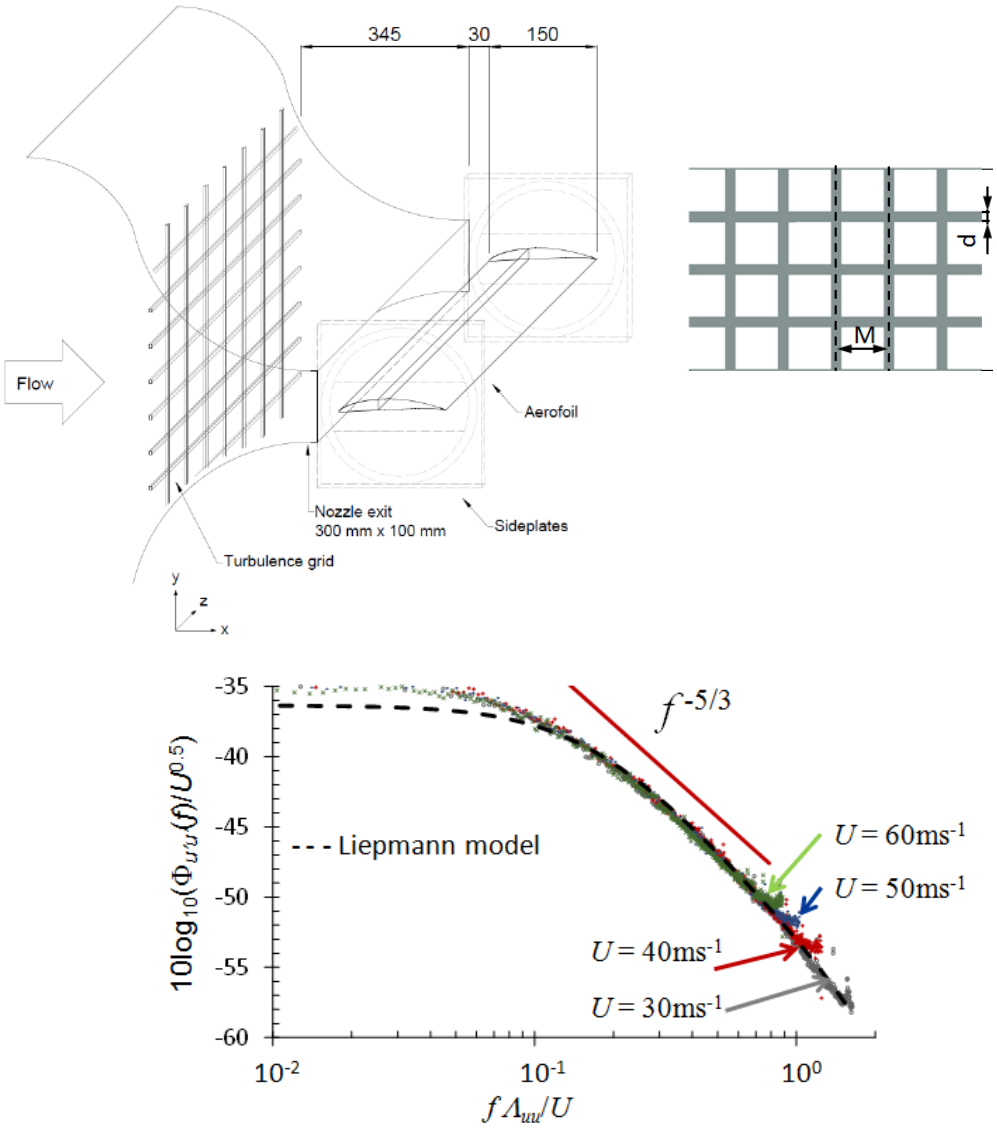

Fig. 3 Isometric drawing of the turbulence grid installed inside the nozzle, definition of the grid parameters and comparison of the normalised one-dimensional turbulence velocity spectra between the Liepmann model and experimental data at $30 \leq U \leq 60$ ms^{-1}.

C. Grid generated turbulence

A woven wire mesh screen is well known for its ability to reduce turbulence intensity and improve flow steadiness. Under normal circumstances, this type of device consists of small mesh length M and wire diameter d. These parameters are depicted in Fig. 3. Some combinations of M and d in a bi-planar grid, as well as the flow velocity, however, can produce exactly the opposite effect: *increasing* the freestream turbulence intensity downstream of the device. A large value of d tends to encourage stronger vortex shedding, thereby increasing the level of turbulence intensity. However, different values of M and velocity with the same d can also produce very different turbulence intensity level, and possibly the integral length scale of the turbulent eddies. Recommendation by Laws and Livesey[14] of a mesh-to-diameter ratio, M/d = 5 for turbulence generated by a bi-planar orthogonal square grid represents a good reference. This criterion is adopted when investigated the noise sources A and D where M = 75 mm and d = 15 mm. The grid is placed inside the nozzle as shown in Fig. 3.

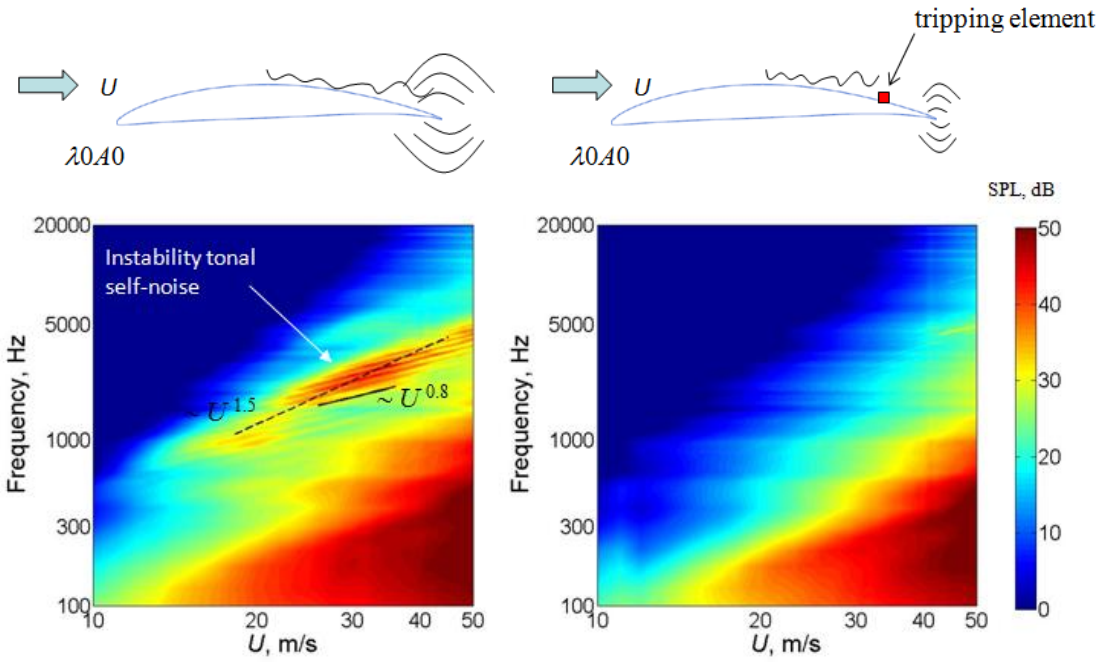

(a)

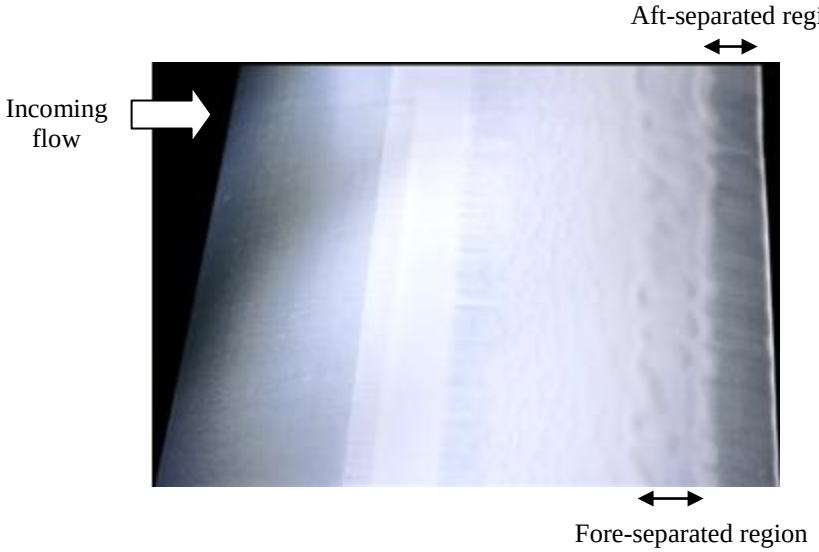

(b)

Fig. 4 (a) SPL (dB, ref. 20μPa) spectra plotted in the frequency–velocity domain for the baseline *λ0A0* aerofoil. Left: clean surface, Right: boundary layer tripping at *x/C* = 0.88 of the suction side, and (b) Surface visualisation for the clean *λ0A0* aerofoil at the suction side. *U* = 24 ms^{-1} and 0^{o} angle of attack.

The decay of the turbulence intensity level in the streamwise distance downstream of the grid, x_l is the function of $(x_l - x_o)^{-5}$, where x_o is the virtual origin of the grid. As a rule of thumb, about twenty times the mesh length M is required to achieve isotropic turbulence behind the grid. This criterion is difficult to be fulfilled in the current setup due to the restrictive geometry between the nozzle exit and the aerofoil model. Hot-wire anemometry was used to examine the isotropy of the grid-generated turbulence. Flow measurement was conducted by a hot wire probe at location near the aerofoil leading edge (without the presence of the aerofoil during the measurement). The measured turbulent velocity power spectral density was then compared with the Liepmann model. The dilution in the high frequency region caused by the Kolmogorov scale is also compensated by applying an exponential function[15]. As

shown in Fig. 3, at flow velocity $30 \leq U \leq 60$ ms^{-1}, the measured streamwise velocity spectra demonstrate -5/3 decay rate and with acceptable agreement to the Liepmann model, except at the low frequency region. The measured streamwise velocity turbulence intensity at location near the aerofoil leading edge is 3.7%, and the integral length scale is about 6.5 mm.

III. (NOISE SOURCE C, Low Freestream *Tu*) Trailing Edge Instability Tonal Noise

This section will present the noise results measured in an aeroacoustic facility when no turbulence grid is installed inside the nozzle. The low turbulence intensity at the freestream ensures that leading edge interaction noise is not the most dominant noise source. The radiated noise from a baseline, straight leading edge aerofoil is mostly originated from the trailing edge, as demonstrated by the Sound Pressure Level, SPL contour map (as a function of frequency and velocity) in Fig. 4a (Left). Several familiar features pertaining to the instability tonal noise produced by a laminar aerofoil are discernible: 1) the existence of velocity scaling laws $\sim U^{1.5}$ and $U^{0.8}$ for the broadband hump and discrete tones, respectively[16–18]; and 2) the existence of the "ladder" structure – the main tone frequencies that initially follow the $U^{0.8}$ scaling would suddenly jump to another parallel curve with the same $U^{0.8}$ dependence. A total of 5 frequency jumps are detected across $10 \leq U \leq 50$ ms^{-1}.

The radiation of the instability tonal noise at the aerofoil trailing edge is only effective when the Tollmien-Schlichting wave is amplified by a laminar separation bubble. The instability tonal noise radiation measured here clearly indicates the presence of a laminar separation region, which is shown by the shaded regions near the suction side trailing edge of the surface flow visualisation in Fig. 4b. From the figure, there is a slight accumulation of the oil mixtures near the separation line due to the near wall reverse flow, thus giving an impression that the aft-separated region is darker than the fore-separated region. For analysis purpose, distinction is given to these separated regions.

Boundary layer trip tape was then placed at $x/C = 0.88$ on the aerofoil's suction side to suppress the laminar separation. The reason to place the trip tape at a relatively downstream location is to ensure that the triggered turbulent boundary layer, if any, will not produce significant broadband noise level at the trailing edge. As shown in Fig. 4a (Right), the instability tonal noise completely disappears when a trip tape is used, therefore re-affirming that the suppression of the laminar separation region near the trailing edge has deprived the amplification process that is required to produce the instability tonal noise.

After the origin of the instability tonal noise has been established, the investigation then focuses on the laminar instability tonal noise subjected to different types of serrated leading edges. Note that the subsequent results presented herein this section are not subjected to artificial boundary layer tripping. Section III.A will discuss the SPL spectra and surface flow visualisation for the same serration amplitude A and different serration wavelength λ. Effect of the same λ and different A to the instability noise will then be examined in Section III.B.

A. Comparison of different λ under the same A

Figure 5a shows the SPL spectra produced by $\lambda 45A7.5$, $\lambda 15A7.5$ and $\lambda 7.5A7.5$. Note that $\lambda 0A0$ is the baseline straight leading edge. An obvious trend discernible in the figure is that, under a same small value of A, the SPL level will reduce when λ decreases. In general, multiple discrete tones are retained for these serrated cases, although the tone frequencies remain unchanged. These behaviours could be explained by the surface flow visualisation results, which were obtained in situ. In Fig. 5b, when λ is the largest, several Ω shape structures are formed at region coincides with the fore-separated region, while the aft region remains fully separated. The combination of these causes the acoustic radiation that still bears the instability tonal noise characteristic, except that the SPL level is now reduced as a result of the Ω structures. For this particular leading edge serration $\lambda 45A7.5$, it is not straightforward to determine the origin of the streamwise vortices from the video footage. However, it has been observed that the trailing edge region that aligns with the serration trough would remain the most resistant to the streamwise vortices. The apex of the Ω structure therefore always aligns with the serration trough at the separation line, where the accumulation of oil mixture that resembles the Ω contour is the footprints of the weakly generated streamwise vortices incapable of propagating further into the aft-separated region, where the flows inside and outside of each Ω structure remain separated. It can be concluded that the successive Ω structures near the trailing edge, which are the remnants of the out of phase flow structures generated by the $\lambda 45A7.5$ serrated leading edge, can slightly disrupt the amplification between the boundary layer instability and the separated flow to cause a reduction in the radiated tonal noise level.

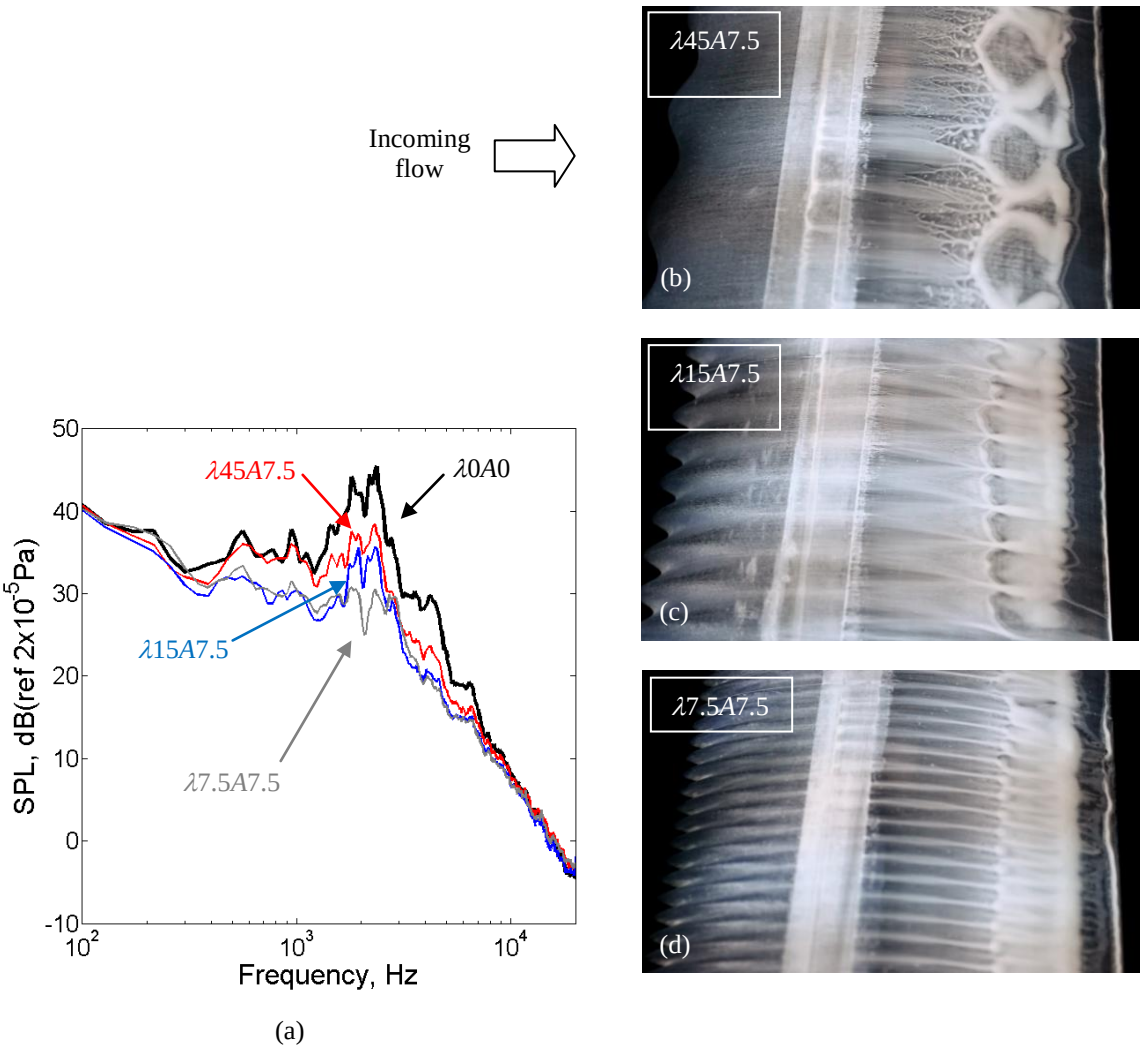

(a)

Fig. 5 See Fig. 7 for caption

Further examination of Fig. 5c, which is the surface flow visualisation result pertaining to the λ15A7.5 narrower serrated leading edge, reveals more structures at the fore-separated region that now resemble succession of "n" shape. Study of the video footage reveals flow movement that could explain the formation of these structures. It is clear that the streamwise vortices were initially emanated from the serration troughs before propagating downstream. These streamwise vortices then split into two smaller vortices at $x/C \approx 0.45$ (close to the start of the adverse pressure gradient at the suction side), before continue to propagate at a large divergence angle away from each other. At a short distance downstream, each of these smaller streamwise vortices will then merge with the neighbouring streamwise vortices originated from other troughs, respectively. Single streamwise vortices will resume after the merging, but they are now out of phase with the serration troughs. Note that the out of phase Ω structures for the λ45A7.5 case discussed earlier is likely to share the same mechanism. The merged streamwise vortices that are now aligned with the serration peak have gained some momentums to penetrate the fore-separated region, but are still unable to enter the aft-separated region. As a result these vortices are entrained back towards the upstream, thus forming the n-shape structures as shown in Fig. 5c. Because there are more streamwise vortices per unit span produced by the λ15A7.5 than the λ45A7.5, it can cause a greater degree of spanwise discontinuity of the separation region. As a result, the radiation of the instability tonal noise will be less efficient, which is manifested in the lower SPL spectrum in Fig. 5a.

The narrowest serrated leading edge λ7.5A7.5, which produces the lowest level of SPL among the three serrated leading edges investigated here, would exhibit a similar "split-and-merge" process for the streamwise vortices described earlier. However, a careful study of the footage reveals that the split-and-merge process has actually

happened twice when reaching the separation line before forming the n-shape structures as seen in Fig. 5d. Similar to the previous cases, the streamwise vortices penetrate well into the fore-separated region, but they are still unable to propagate beyond and into the aft-separated region. However, the total separated area that has been encompassed by the streamwise vortices is the largest for the $\lambda 7.5A7.5$ serrated leading edge. Therefore the reduction of the tonal noise level is also quite significant in this case.

As a summary for the effect of serration wavelength λ on the instability tonal noise, it is found that a smaller λ (narrower serration) can reduce the tonal noise level further. This is because a narrower serration can produce more streamwise vortices per unit span that would encompass a larger area of the separated region near the trailing edge, which subsequently weakens the amplification process that is needed to sustain the radiation of instability tonal noise. However, the three serrated leading edges investigated here all have small value of serration amplitude A, therefore only weak spanwise pressure gradient exists near the leading edge[10]. This may deprive the formation of a strong streamwise vortical system that can otherwise be produced by a serrated leading edge with large serration amplitude A.

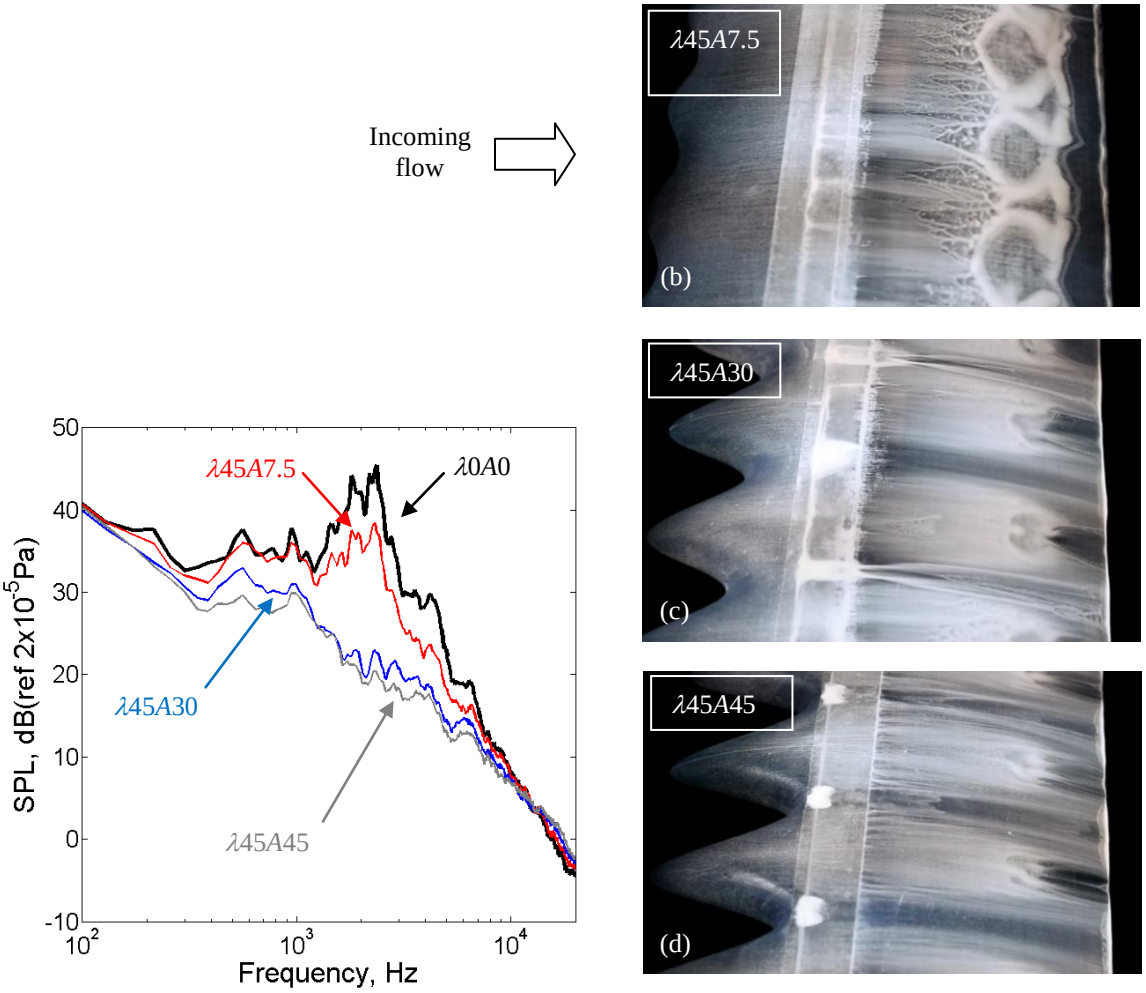

(a)

Fig. 6 See Fig. 7 for caption

B. Comparison of different *A* under the same λ

This section investigates the effect of serration amplitude A on the instability tonal noise radiation. Figure 6a shows the SPL spectra produced by $\lambda 45A7.5$, $\lambda 45A30$ and $\lambda 45A45$ serrated leading edges. From the figure, it is clear

that the radiated noise is more sensitive to A, where the level of reduction in the instability tonal noise can be improved significantly when A increases. A complete suppression of the instability tonal noise up to 25 dB can be achieved by the $\lambda 45A45$ case. From the figure, the A should be at least 30 mm (or $A/C \approx 0.2$) to cause a complete loss in the instability tonal noise characteristics (broadband tonal hump and multi-discrete tones).

The surface flow visualisation results are again examined in order to determine the underlying mechanism. As already discussed in the previous section, the $\lambda 45A7.5$ serrated leading edge is the least efficient configuration to suppress the instability tonal noise. The corresponding surface oil flow pattern is reproduced in Fig. 6b for the purpose of comparison. For the $\lambda 45A30$ case, where the serration amplitude A is relatively large, a significant suppression of the tonal noise has been achieved. The acoustic result in this case is corroborated by the corresponding surface oil flow pattern in Fig. 6c, where strong streamwise vortices are shown to emanate from the serration troughs and penetrate deep into the trailing edge. In the absence of the split-and-merge process for the streamwise vortices in this case, they are all in phase with the serration troughs. The Ω structures at the fore-separated region are now in phase with the serration peaks and trapped between the streamwise vortices. Note that the Ω structures produce by the $\lambda 45A30$ serrated leading edge are more slender in size compared to the $\lambda 45A7.5$ case, despite both share the same serration wavelength λ. There is a large difference in the acoustic spectra between the $\lambda 45A7.5$ and $\lambda 45A30$ serrated leading edges. The reason is that the $\lambda 45A30$ serrated leading edge produces

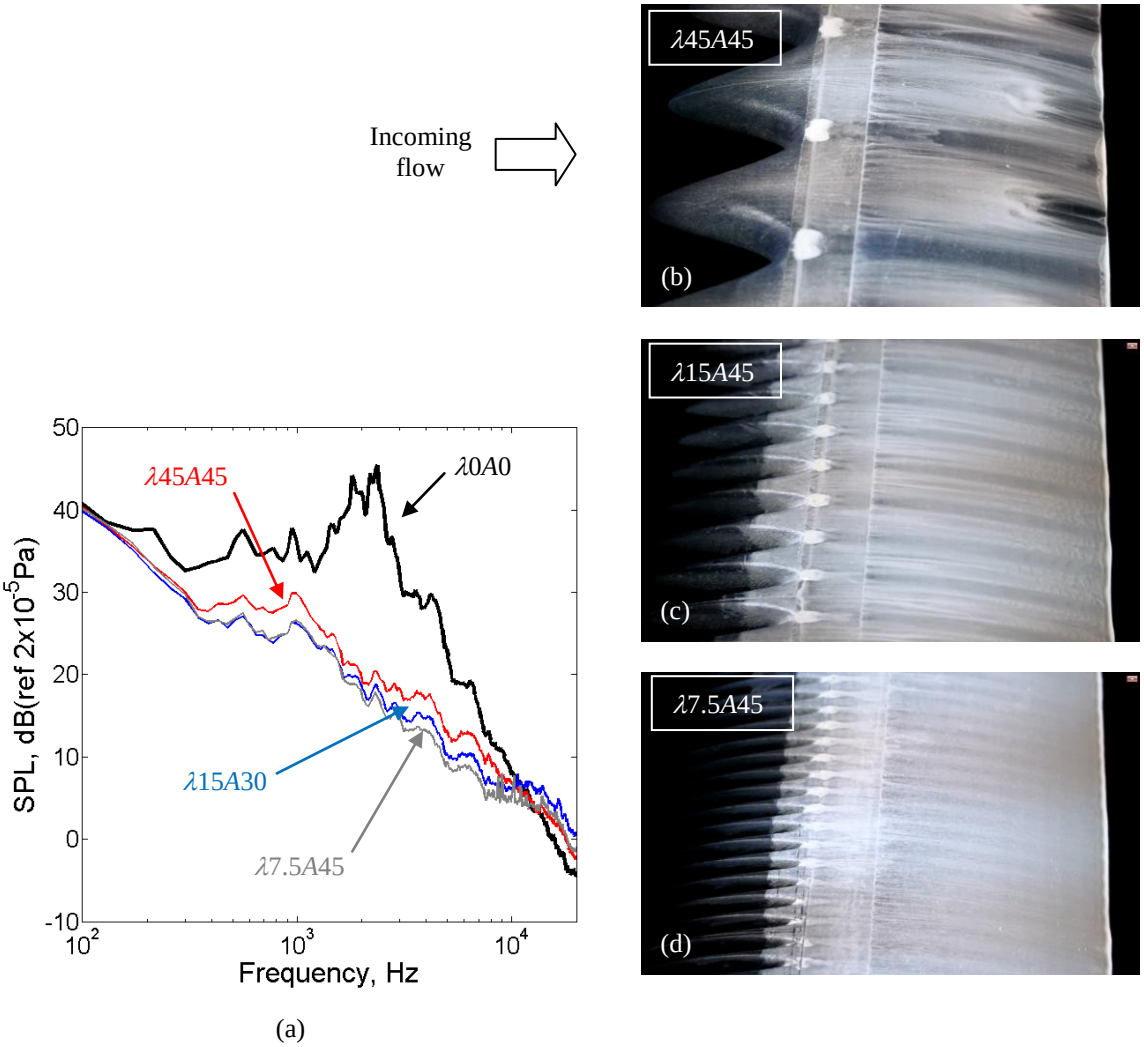

(a)

Fig. 7 (a) SPL (dB, ref. 20μPa) spectra for the instability tonal noise by different leading edges, and (b–d) Surface visualisations measured simultaneously with the noise. No boundary layer trip tape on the surface. U = 24 ms^{-1} and 0^{o} angle of attack.

stronger streamwise vortices that are capable of penetrating into the aft-separated region close to the trailing edge. This is a significant improvement over the $\lambda 45A7.5$ case where the aft region remains separated across the whole span.

When the serration amplitude is further increased to $\lambda 45A45$, pockets of oil mixture are accumulated at the vicinity of the serration troughs in Fig. 6d. Each of these pockets consists of two recirculating cells where one rotates clockwise, and another one anti-clockwise. These recirculating cells seem to encourage the generation of large streamwise vortices with a higher momentum, as manifested by the even more slender Ω structures amongst the array of the streamwise vortices. Because the $\lambda 45A45$ serrated leading edge can produce flow structures that suppress a larger portion of the separated region near the trailing edge, a slight improvement in the tonal noise reduction can be observed in Fig. 6a.

The results presented thus far for the $\lambda 45A7.5$, $\lambda 15A7.5$, $\lambda 7.5A7.5$, $\lambda 45A30$ and $\lambda 45A45$ serrated leading edges allow us to establish that small λ and large A are the prerequisites for an effective reduction of the instability tonal noise. The underlying mechanism is the generation of more high-momentum streamwise vortices per unit span to suppress the laminar separation region near the trailing edge. It will be of interest to examine the acoustic radiation and the surface flow visualisation produced by serrated leading edges with the smallest λ and largest A. Figure 7a compares the SPL spectra produced by the $\lambda 45A45$, $\lambda 15A45$ and $\lambda 7.5A45$ cases. The corresponding surface oil flow patterns are also shown alongside for comparison (Fig. 7b–d, respectively). Note that these three serrated leading edges have the same largest A, but different λ. In accordance to the trend, further reduction of the radiated noise level is observed when λ reduces, where the largest level of noise reduction is achieved by the $\lambda 7.5A45$ serrated leading edge. The corresponding surface oil flow pattern in Fig. 7d reveals that the streamwise vortices generated by the $\lambda 7.5A45$ serrated leading edge have removed the separated flow structures (Ω, n) that were otherwise present near the trailing edge. In Fig. 7c for the intermediate wavelength $\lambda 15A45$, the surface flow pattern demonstrates a partial suppression of the separated flow structures, where the radiated noise is slightly higher than the $\lambda 7.5A45$, but still significantly lower than the $\lambda 45A45$.

It should be mentioned that some high frequency (f > 10 kHz) noise increases occurs when A increases. Although the current single microphone configuration cannot identify the exact noise source, it can be conjectured that the high frequency noise is the result of leakage noise through the large serration gaps (as the result of large A) at the leading edge.

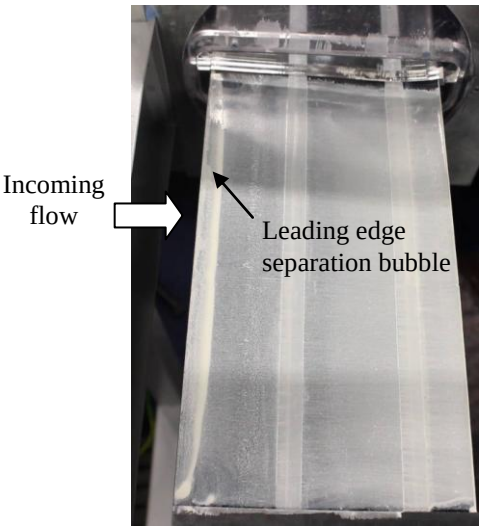

Fig. 8 Aerofoil pressure side oil flow visualisation to detect the leading edge separation bubble. U = 24 ms^{-1} and 0^{o} angle of attack.

IV. (NOISE SOURCE B, Low Freestream *Tu*) Leading Edge Separation Bubble Noise

This section will investigate the role of leading edge separation bubble on the noise radiation, and how a serrated leading edge could be used to suppress it. The existence and extent of the separation bubble on the NACA 65(12)-10 needs to be ascertained first. Moreover, it is also necessary to establish the frequency range in the acoustic spectrum within which the separation bubble noise is dominant.

The same oil flow technique in Section III is repeated here for the detection of the leading edge separation bubble at the pressure side based on examination of the oil residue footprint. Set at 0 degree angle of attack and U = 24 ms^{-1}, Fig. 8 demonstrates clear division lines at the pressure side between $0 \le x/C \sim< 0.17$ for the $\lambda 0A0$ baseline case, thus confirming the existence of separation bubble at the leading edge. For the investigation of the separation bubble noise, Fig. 9a illustrates the aerofoil setup for the baseline $\lambda 0A0$ leading edge: at the aerofoil's suction side, a trip tape is permanently placed at x/C = 0.33 from the leading edge to trigger a bypass transition and remove the instability tonal noise that will otherwise be radiated at the trailing edge. At the pressure side, the same grade of trip tape is placed sequentially across 6 locations: x/C = 0.03, 0.07, 0.13, 0.2, 0.27 and 0.33, during which far field acoustic measurement is performed for each case. Figure 9b shows the aerofoil setup when the leading edge is replaced with the $\lambda 26A45$ serrated type. Here the trip tape at the suction side remains the same as above, but at the

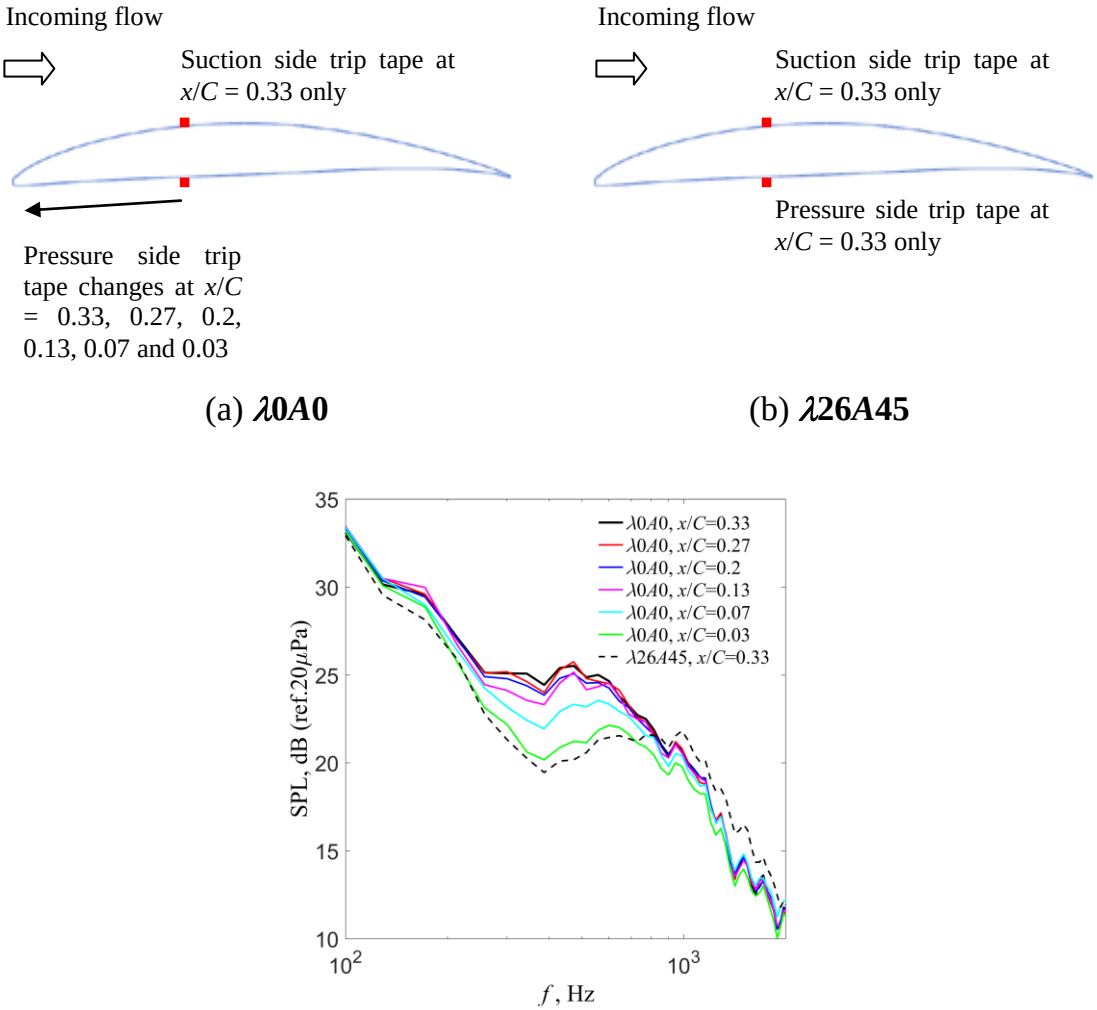

Fig. 9 Schematics explaining the different locations of trip tapes for the (a) $\lambda 0A0$, (b) $\lambda 26A45$ aerofoil. (c) Comparison of SPL for different trip locations on the aerofoil and their implications to the separation bubble noise. U = 24 ms^{-1} and 0^{o} angle of attack. First element of the legend refers to the type of leading edge used, and the second element refers to the trip location at the pressure side. Trip location at the suction is always at x/C = 0.33.

pressure side the trip tape is only placed at x/C = 0.33, i.e. slightly downstream of the serration troughs. All the measured far field PSDs are shown in Fig. 9c.

While the flow visualisation in Fig. 8 proves the existence of a leading edge separation bubble at the pressure side of the NACA 65(12)-10, the acoustic results in Fig. 9c provide further evidences that the bubble is an effective noise source at low frequency. With the limited data available here, and assuming that the trip tape can force instantaneous bypass transition but has no influence on the flow upstream, it seems that the level of the separated noise can be related to the bubble length. When the trip tape is placed downstream of the separation bubble, i.e. $x/C \geq 0.20$ at the pressure side of the $\lambda 0A0$ straight leading edge, a broadband hump takes a prominent presence in the acoustic spectra at $250 \leq f \leq 900$ Hz. When the trip tape is placed within the bubble, e.g. at x/C = 0.07, noise radiation due to separation bubble becomes weaker. When turbulent boundary layer is formed at the vicinity of the leading edge (i.e. trip tape at x/C = 0.03), it is believed that no bubble could exist and this is collaborated by the almost disappearance of the broadband hump.

When the leading edge is replaced with the $\lambda 26A45$ serrated type, where the trip tape at the pressure side is now placed at x/C = 0.33, the disappearance of the broadband hump is in stark contrast with the $\lambda 0A0$ baseline for the same trip location, which shows a prominent presence of the broadband hump. This demonstrates that the leading edge serration can be an effective control device for the reduction of leading edge separation bubble noise.

As shown in Fig. 9b for the setup, combination of the leading edge serration and both the trip tapes at the suction and pressure sides will result in the absence of instability tonal noise and separation bubble noise in the acoustic spectra. Furthermore, low turbulence intensity in the free jet also means that the turbulence–leading edge interaction noise will not be significant. Therefore, noise sources contributing to the acoustic spectrum in Fig. 9c for the $\lambda 26A45$ serrated leading edge are mainly made up by the trailing edge self-noise, background noise and jet noise. Interestingly, noise increase by the $\lambda 26A45$ serrated leading edge can be observed at $900 \leq f \leq 2000$ Hz. This implies that the secondary/vortical flows generated by the serration, after convecting to the trailing edge and interacting with the local turbulent boundary layer, could become a new source of noise radiation.

V. (NOISE SOURCE A, Elevated Freestream *Tu*) Leading Edge-Turbulence Interaction Broadband Noise

This section concerns the case when the turbulence grid described in Section II.C is installed inside the nozzle. Note that trip taps were not employed on the aerofoil surface in this study. Despite the absence of the trip tape, the investigation of the turbulence–leading edge interaction noise can still be undertaken because the presence of the elevated freestream turbulence intensity as a result of the turbulence grid can encourage bypass transition of the boundary layer in almost the same way as placing tripping element on the aerofoil surface. Therefore, turbulent boundary layer can be generated at the trailing edge, where the radiated noise at the trailing edge will not bear the tonal characteristic anymore. Instead it will become more broadband in characteristic.

The values of λ investigated in this study are 7.5, 15, 30 and 45 mm, which give λ/C = 0.05, 0.1, 0.2 and 0.3, respectively. A similar range also applies to the amplitude where A/C = 0.05, 0.2 and 0.3.

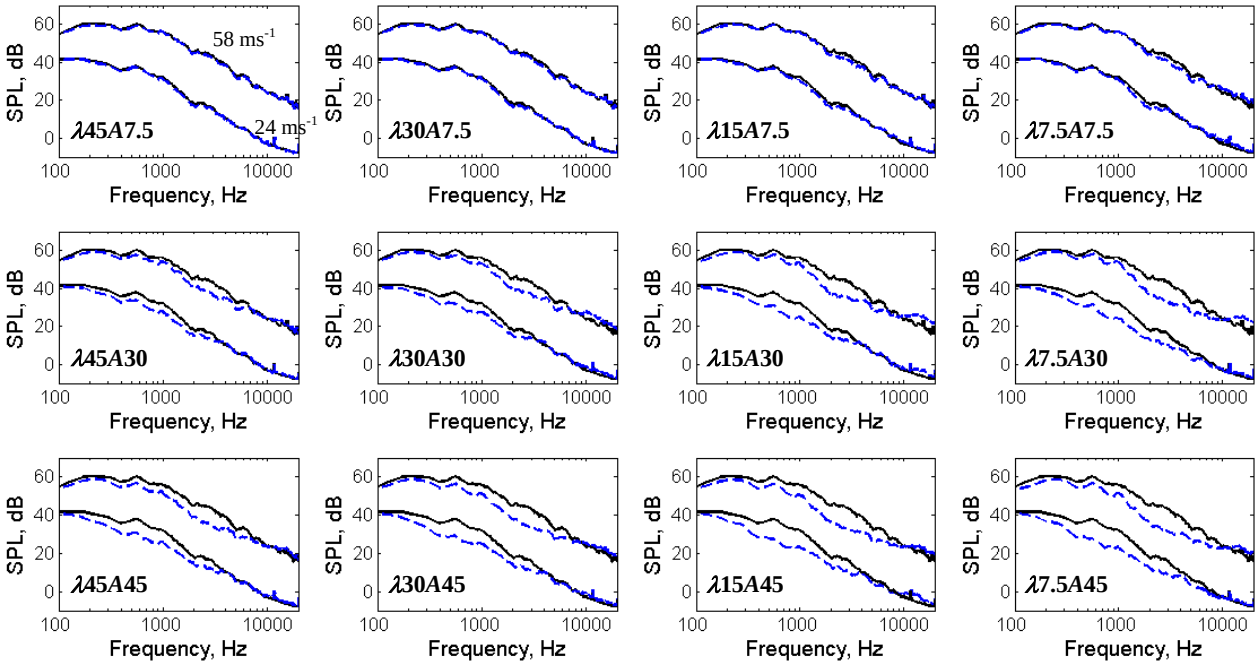

Fig. 10 Comparisons of SPL (dB, ref. 20μPa) for the turbulence–leading edge interaction noise at U = 24 ms^{-1} and 58 ms^{-1} produced by (—) baseline leading edge $\lambda 0A0$, and (– – –) serrated leading edges of different λ and A. The aerofoil is set at 0 degree angle of attack.

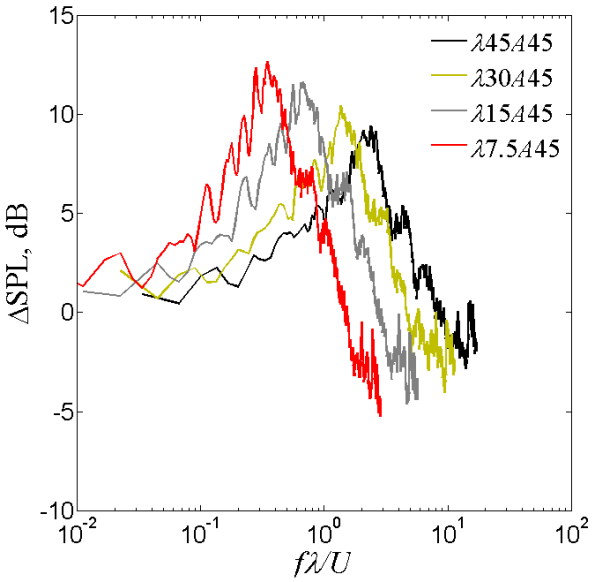

Fig. 11 Spectra of ΔSPL, dB (turbulence–leading edge interaction noise reduction) at U = 58 ms^{-1} and 0 degree angle of attack, with the frequency scaling of $f\lambda/U$.

A. Parametric study of the effect of λ and A on the interaction noise radiation

Figure 10 compares the SPL spectra for the 12 serrated leading edges against the baseline $\lambda 0A0$ at U = 24 and 58 ms^{-1}. Examination of the SPL spectra produced by the $\lambda 0A0$ case, which are broadband in nature, confirms that the main noise source is now the turbulence–leading edge interaction noise. It is believed that the elevated freestream turbulence intensity has triggered a bypass transition on the aerofoil surface because there is a clear absence of any tonal components in the acoustic spectra.

Introducing various degrees of λ and A to the serrated leading edges can produce very different characteristics of the interaction noise. The noise performance improves slightly as λ decreases. However, the most straightforward way to achieve significant reduction in the leading edge interaction noise is to increase the value of A. The $\lambda 7.5A45$ serrated leading edge (smallest wavelength and largest amplitude) produces the largest level of noise reduction. On the opposite end, the $\lambda 45A7.5$ serrated leading edge (largest wavelength and smallest amplitude) would produce the SPL spectra that are almost identical to the baseline aerofoil ($\lambda 0A0$).

The next step is to investigate the dependence of the interaction noise reduction, as a function of the frequency, on these serration parameters. A straightforward representation of the interaction noise reduction is ΔSPL, which is the difference in SPL produced by the aerofoil with leading edges between a straight one ($\lambda 0A0$) and a serrated one. Positive values of ΔSPL denote noise reduction by the serration, and a negative ΔSPL means that the serration produces higher noise level than the baseline case. Figure 11 presents the ΔSPL spectra with non-dimensional frequencies of $f\lambda/U$ at U = 58 ms^{-1} for the $\lambda 45A45$, $\lambda 30A45$, $\lambda 15A45$ and $\lambda 7.5A45$ serrated leading edges, which clearly show that the curves fail to collapse. This is consistent with the earlier observation that the serration wavelength is not the most dominant parameter for the ΔSPL.

Rather, the use of serration amplitude as a scaling parameter is found to provide a good level of collapse for the curves. It is also found that the serration wavelength λ can affect the gradient of the ΔSPL spectra slightly. Effort is then made to include the serration wavelength λ into the definition of the non-dimensional frequency. After examining the available data set, an empirical relationship is suggested:

$$\Delta\mathrm{SPL} = Gf', \quad \text{where} \quad \begin{pmatrix} G = 7.8\,\exp\left(-1.5\mu.\mathrm{Re}\right) \\ f' = \dfrac{fA}{U}\left(\dfrac{\lambda}{C}\right)^{-0.3} \end{pmatrix} \tag{1}$$

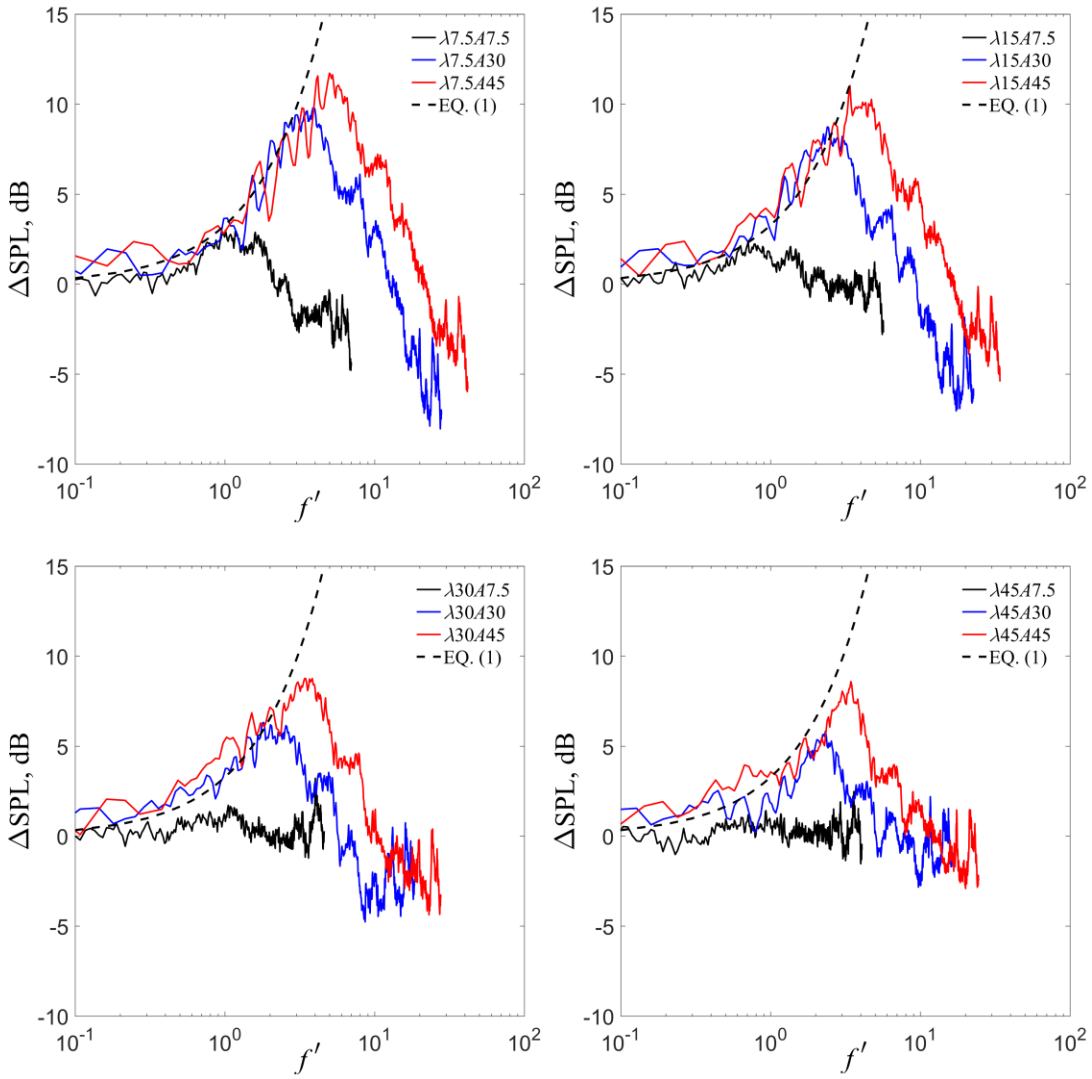

Fig. 12 Spectra of ΔSPL, dB (turbulence–leading edge interaction noise reduction) at U = 58 ms^{-1} and 0 degree angle of attack, with the frequency scaling of $f' = fA/U.(\lambda/C)^{-0.3}$

Figure 12 shows the ΔSPL spectra scaled with the non-dimensional frequency f' at U = 58 ms^{-1}. Generally, the ΔSPL spectra exhibit a "convex" shape. This means that the ΔSPL initially increases as the frequency increases, before it reaches the main peak (ΔSPL_{peak}) that usually sustains over a finite frequency range. The non-dimensional frequency corresponds to ΔSPL_{peak} is represented by f'_{peak}. EQ. (1) is found to be universal and can predict well the ΔSPL, although it is only valid at $0 \leq f' \leq f'_{peak}$. At $f' > f'_{peak}$, the ΔSPL will start to decay with the presence of several sub-peaks.

So far the analysis only focuses on a single velocity at U = 58 ms^{-1}, where the largest ΔSPL_{peak} (~13 dB) is achieved by the λ7.5A45 case, i.e. the largest serration amplitude combined with the smallest serration wavelength. To determine whether this remains true for other velocities or Reynolds numbers, one could examine the ΔSPL contour maps as a function of f' and U. The collection of ΔSPL contours in Fig. 13 clearly supports the above pre-requisite in the serration geometries for achieving high ΔSPL across the whole range of velocities. It is interesting to note that noise increase (ΔSPL < 0) occurs at very high frequency for some cases. The magnitude of the noise increase at high frequency depends upon the serration parameters, which can be enhanced by small serration

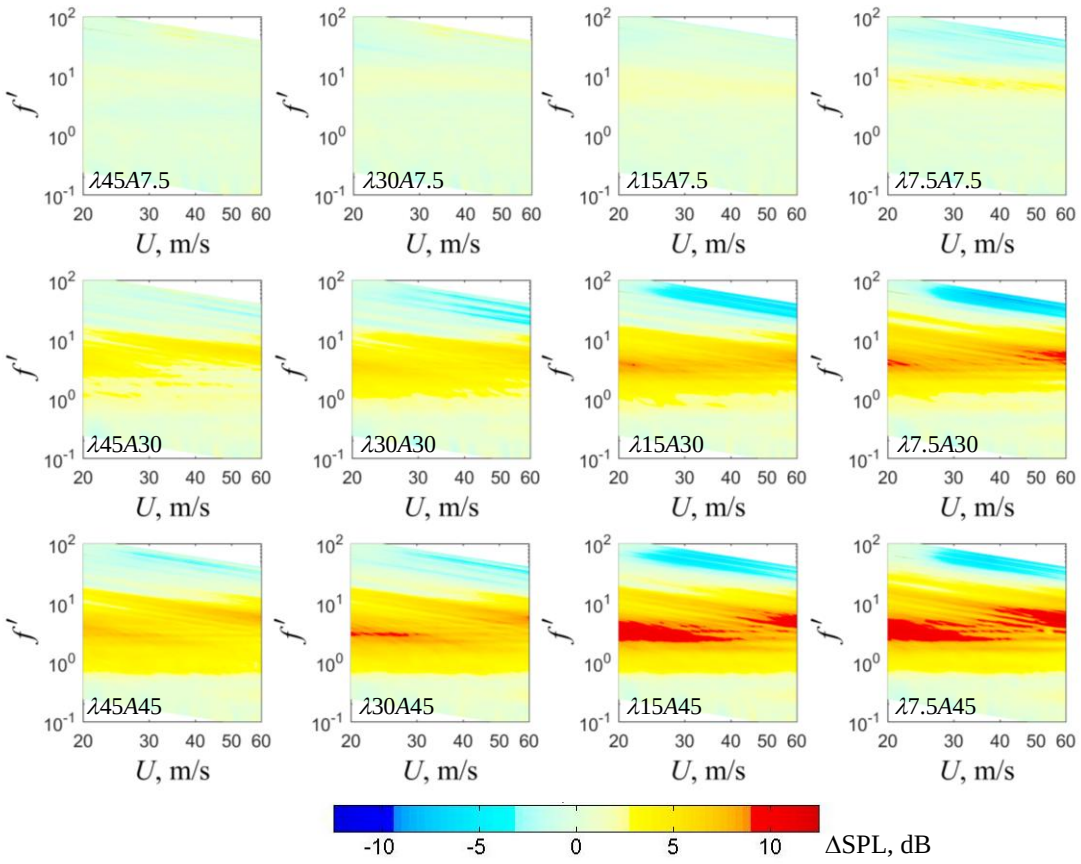

Fig. 13 Contour maps of ΔSPL, dB (turbulence–leading edge interaction noise) as a function of f' and U for different serrated leading edges. The aerofoil is set at 0 degree angle of attack.

wavelength λ and large serration amplitude A. Such combination of the serration parameters can promote the fluid–structure interaction within the serration gaps that potentially acts as a superfluous noise source.

The Overall Sound Pressure Level, OASPL is another useful acoustic term to quantify the noise reduction performances of the serrated leading edges. Figure 14a shows the variation of OASPL with U for the $\lambda 0A0$ (baseline), $\lambda 7.5A7.5$, $\lambda 7.5A30$ and $\lambda 7.5A45$ serrated leading edges. Note that when integrating the mean square acoustic pressure to obtain the OASPL, the lower and upper limits of the frequencies are 50 and 20,000 Hz, respectively. For the $\lambda 0A0$ baseline leading edge, dipole radiation of the turbulence–leading edge interaction noise is found to be dominant with a velocity dependence of OASPL $\propto U^{5.5}$. For the three serrated leading edges, a similar velocity power law also applies despite the radiation of consistently lower level of OASPL. This indicates that although the serration can reduce the magnitude of the leading edge noise, it cannot completely destroy the source at the trough region (to be discussed in Section V.B). This provides scope for further reduction of the magnitude of the leading edge noise if additional source control measure applies to the trough region of a serrated leading edge. For example, Chaitanya[19] observed a further reduction in the leading edge noise when cut-in slots applies to the serration troughs.

Bar chart of ΔOASPL, which is defined as the difference in OASPL produced by the aerofoil with the $\lambda 0A0$ baseline leading edge and a serrated leading edge, is shown in Fig. 14b for U = 58 ms^{-1}. Similar to the earlier observations, though the ΔOASPL is the most sensitive to the serration amplitude A, it also exhibits a preference to small serration wavelength λ. Interestingly, when comparing the two smallest serration wavelengths of λ/C = 0.05 and 0.1 (7.5 and 15 mm, respectively), the result also suggests that the ΔOASPL pertaining to the λ/C = 0.05 is somehow lower than those produced by the λ/C = 0.1. The reason is that noise increase at high frequency is also prominent when λ is small (e.g. see Fig 13). This inevitably counteracts the good level of reduction in the turbulence–leading edge noise achieved at lower frequency.

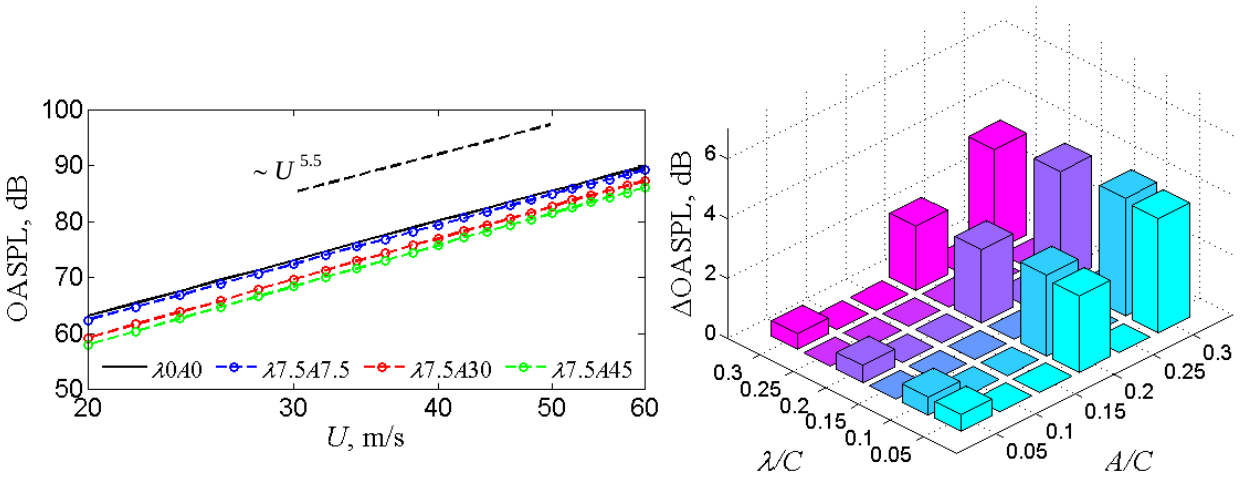

(a) (b)

Fig. 14 (a) Variations of OASPL with *U* for several leading edges, including the baseline *λ0A0*, and (b) Bar chart of ΔOASPL, dB (turbulence–leading edge interaction noise reduction) for the serrated trailing edges at *U* = 58 ms^{-1}. The aerofoil is set at 0 degree angle of attack.

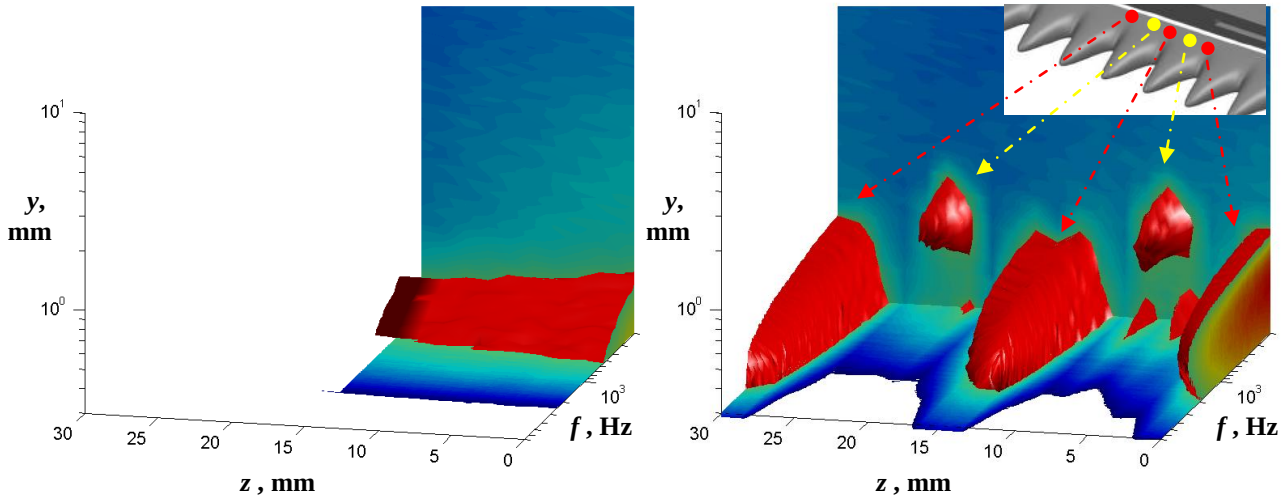

Fig. 15 Power Spectra Density of the streamwise boundary layer fluctuating velocity measured at *x/C* = 0.3, under *U* = 24 ms^{-1} and 0 degree angle of attack. The threshold to separate the turbulent and non-turbulent interface is the same for both the *λ0A0* and *λ15A45* aerofoil.

B. Supplementary boundary layer measurement

It has now been well established that serrated leading edge is a very effective device to reduce the turbulence–leading edge interaction broadband noise. For an optimal ratio between the serration wavelength and the incoming turbulence integral length scale (roughly equal to 4 according to Chaitanya[19]), Kim et al.[10] suggest that for a particular turbulence eddy the first point of contact to the aerofoil will be the most protrude part of the serration (peak). Continuous interaction between the remaining part of the turbulence eddy and the aerofoil body will take place along the oblique edge until the serration trough. If noise is radiated whenever there is a contact taking place

between the eddy and aerofoil surface, the serration essentially acts as a "phase-lag" device to offer destructive-interference of the acoustic disturbances. Kim et al.[10] also point out that the remaining contributor to the interaction noise radiation for a serrated leading edge is related to the flow dynamics at the serration trough region.

In the current study, an attempt is made to supplement the above acoustical mechanism from a hydrodynamic perspective. It is not easy to measure the turbulent flow within the serration gap using hot-wire. Instead, the focus is placed on the PSD of the boundary layer fluctuating velocity in a y–z plane immediately downstream of the serration trough. The $\lambda 15A45$ serrated leading edge, which has earlier been shown as one of the best serration configurations for the reduction of interaction noise, is chosen for this study. Figure 15 shows the PSD of the streamwise fluctuating velocity in a y–z–f domain produced by both the $\lambda 0A0$ and $\lambda 15A45$ leading edges at $x/C \approx 0.3$, $U = 24$ ms^{-1} and 0 degree angle of attack. Note that $x/C \approx 0.3$ for the $\lambda 15A45$ serrated leading edge corresponds to the streamwise location immediately downstream of the serration troughs. Figure 15 aims to demonstrate the change in boundary layer turbulent characteristics following the interaction between the incoming turbulent flow and baseline/serrated leading edges. Although the threshold level used to separate the turbulent and non-turbulent interface in the PSD is arbitrarily chosen, the turbulence structures (i.e. regions of high PSD level for the fluctuating velocity) should still be portrayed reasonably well in this presentation. For consistency, the same threshold level is adopted for both types of leading edges.

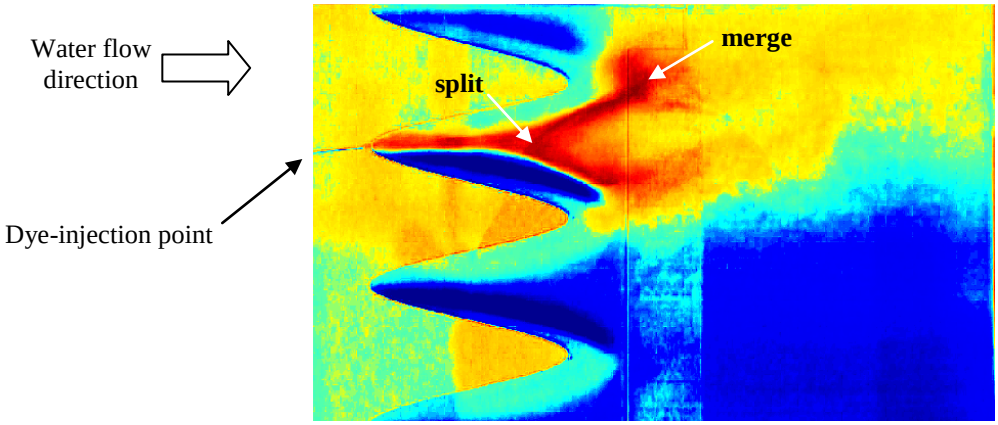

Fig. 16 Top view of a time-averaged "Saturation" image for the $\lambda 15A45$ aerofoil subjected to colour dye-injection slightly upstream to one of the serration peaks in a water tunnel. A total of about 300 images were used for the averaging during image processing.

It can be seen that turbulence structures produced by the $\lambda 0A0$ and $\lambda 15A45$ leading edges are markedly different between each other. For the $\lambda 0A0$ leading edge, region of high PSD for the fluctuating velocity is relatively thin in the wall-normal direction, but is consistent across the spanwise z-direction. However, for the $\lambda 15A45$ serrated leading edge, boundary layers behind the serration peaks and serration troughs paint a different picture. The turbulence structures become less significant and even lifted up from the wall at spanwise locations that align with the serration peaks. This could give an impression that the incoming turbulent flow does not impinge the serration peaks directly, thereby resulting in a lower degree of interaction noise radiation locally. To investigate this further, the aerofoil was taken to a water tunnel for dye-flow visualisation. Figure 16 shows the top-view of the aerofoil in a time-averaged "saturation" map when one of the serration peaks is subjected to dye-flow injection. It can be seen that the time-averaged dye does not separate at the serration peak, but remains attached along the sawtooth. This indicates that flow interaction on the serration peak does indeed occur. However, it would suddenly undergo a splitting process at some points downstream. After the splitting, most of the dye would converge to the adjacent serration troughs, while some are lifted up from the surface. Now referring back to Fig. 15, behind each serration trough large cigar-shaped turbulence structure can be seen extending to higher frequency. These enhanced turbulence structures corroborate well with the dye-visualisation in Fig. 16, and the earlier oil flow visualisation results.

The results in Figs. 15 and 16, which only focus on the suction side of the aerofoil, indicate that the flow dynamics downstream of the serrated leading edge can become very three-dimensional and difficult to predict. The flow dynamics at the pressure side can also be equally complex. The combination of both might have some

implications to the self-noise radiation when they reach the trailing edge. This issue will be investigated in the next section.

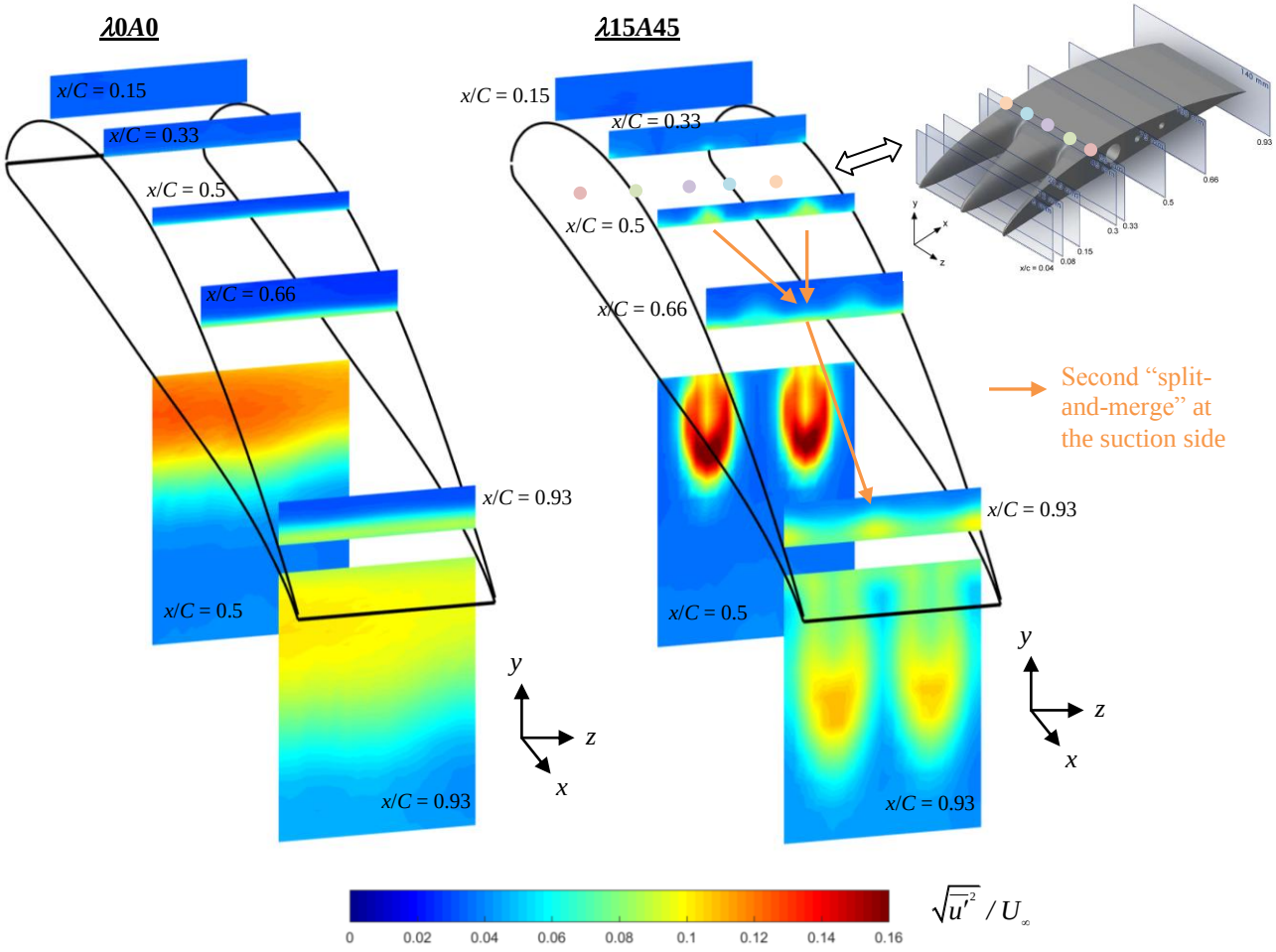

Fig. 17 Distribution of the boundary layer turbulence intensity $\sqrt{\overline{u'^2}} / U_\infty$ on the suction and pressure sides of the aerofoil when subjected to the $\lambda 0A0$ baseline and $\lambda 26A45$ serrated leading edges at U = 24 ms^{-1} and 0 degree angle of attack.

VI. (NOISE SOURCE D, Elevated Freestream *Tu*) Trailing Edge Turbulent Broadband Self-Noise: implications and challenges

The $\lambda 26A45$ serrated leading edge investigated here has a slightly wider wavelength than the previous one, but the amplitude is the same. Boundary layer velocity measurements in y–z plane are performed at x/C = 0.15, 0.33, 0.5, 0.66 and 0.93 for the suction side, and x/C = 0.5 and 0.93 for the pressure side of the aerofoil. Very near wake measurement in y–z plane at x/C = 1.02 is also performed. No trip tape is used on the aerofoil surfaces, and the aerofoil angle of attack remains the same at 0 degree and the jet velocity U = 24 ms^{-1}.

Figure 17 compares the distributions of the turbulence intensity $\sqrt{\overline{u'^2}} / U_\infty$ for the turbulent boundary layers developed on the suction and pressure sides of the aerofoil when subjected to the $\lambda 0A0$ and $\lambda 26A45$ leading edges. u is the streamwise component of the velocity, u' refers to the streamwise velocity fluctuation and U_∞ is the local freestream velocity. These quantities are measured by a boundary layer type single hot wire probe. For the straight $\lambda 0A0$ case, the growth of the turbulent boundary layer is more prominent at the pressure side than at the suction side, which is consistent to the fact that adverse pressure gradient covers almost the entire pressure surface of the aerofoil.

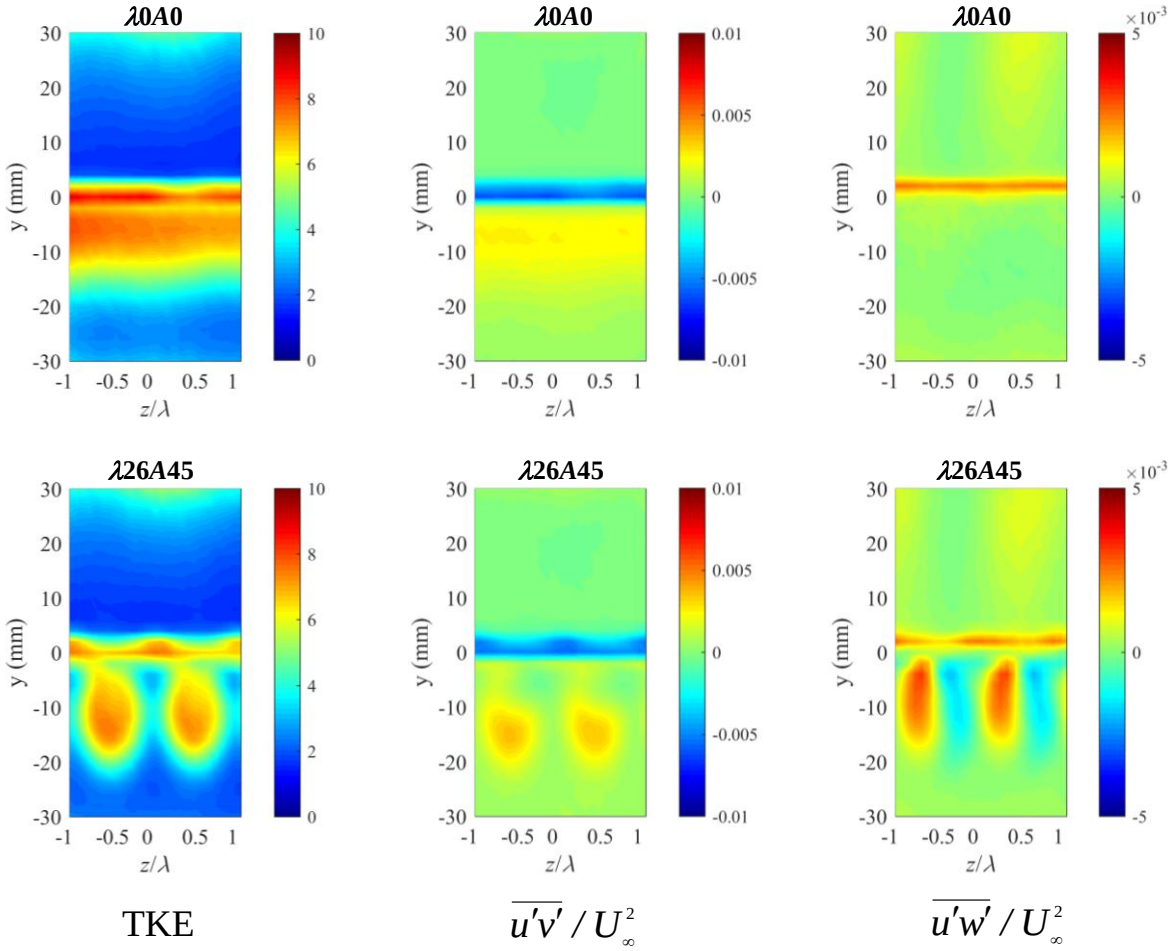

Fig. 18 Comparison of the TKE, $\overline{u'v'}/U_\infty^2$ and $\overline{u'w'}/U_\infty^2$ of the very near wake (*x*/*C* = 1.02) produced by aerofoil with either the *λ*0*A*0 baseline or the *λ*26*A*45 serrated leading edges. Suction is located at *y* > 0, and pressure side at *y* < 0. *U* = 24 ms^{-1} and 0 degree angle of attack.

At *x*/*C* = 0.5, when a serrated leading edge is used, there is a prominent region of laminar flow between two "fingers" of highly turbulent regions (originated from the serration troughs). This suggests that the secondary flow that forms the fingers, which is later to be shown as a pair of streamwise vortices, can entrain the surrounding shear flow and re-laminarise the surrounding otherwise turbulent boundary layer in the process. The very high turbulence intensity within the fingers seems to be lifted up away from the wall, and this trend continues down to the trailing edge at *x*/*C* = 0.93. As far as the near-wall region at the pressure side trailing edge is concerned for the *λ*26*A*45 aerofoil, the turbulence level is significantly lower than that produced by the baseline *λ*0*A*0 leading edge aerofoil.

Boundary layer at the suction side, on the other hand, is first subjected to streamwise favourable pressure gradient up to at least mid-chord of the aerofoil. From then on the adverse pressure gradient will become dominant down to the trailing edge. High turbulence intensity regions are originally produced at the serration troughs after subjecting to the first "split-and-merge" process (see Fig. 16). However, as the enhanced turbulent flow propagates downstream, they appear to exhibit a second "split-and-merge" (*x*/*C* = 0.5→0.93). This means that high turbulence intensity now accumulates at the spanwise location that is only aligned with the leading edge serration peaks.

In summary, the above flow characteristics will result in two scenarios at the trailing edge: (1) periodic lifting of high turbulent fluids at the pressure side, and they only align with the serration troughs across the span, and (2) the two "split-and-merge" processes at the suction side enable the return of the high turbulent fluids to the locations that only align to the serration peaks across the span. The combination of the two scenarios above will cause a mismatch (out-of-phase) of prominent turbulent fluids between the suction and pressure sides near the trailing edge. More

importantly, the existence of periodic turbulent fluids across the span for both the suction and pressure sides equally implies that periodically laminarised fluids are also present near the trailing edge.

More insight of the turbulent, or vortical structures could be gained if the velocity components in the vertical v and spanwise w directions are also available. Using X-wire probe (and by rotating the probe in 90° to switch the measurement of the velocities from (u & v) to (u & w), or vice versa), Fig. 18 compares the Reynolds shear stresses in $\overline{u'v'}/U_\infty^2$ and $\overline{u'w'}/U_\infty^2$, as well as the turbulent kinetic energy TKE $0.5\left(\overline{u'^2}+\overline{v'^2}+\overline{w'^2}\right)$ at the very near wake (x/C = 1.02) produced by the $\lambda 0A0$ and $\lambda 26A45$ aerofoil. It is very clear that distribution of the TKE, which can represent footprint of the upstream boundary layers, is heavily modulated when subjected to the serrated leading edge. There also appears to contain many low-turbulent energy pockets embedded within the wake flow. The out-of-phase turbulent fluids between the suction and pressure sides, as described earlier in the boundary layer results, is also evident here. The distribution of the TKE largely corroborates with the Reynolds shear stress $\overline{u'v'}/U_\infty^2$ for both the $\lambda 0A0$ and $\lambda 26A45$ aerofoil. Based on the coordinate system adopted here, turbulent boundary layer on the aerofoil pressure side that undegoes turbulence transport events such as ejection of the near wall low-speed fluid ($u' < 0$, $v' < 0$), or sweeping of high-momentum flow towards the wall ($u' > 0$, $v' > 0$), will predominantly return positive value for the Reynolds shear stress $\overline{u'v'}/U_\infty^2$. Indeed this reflects very well in the $\lambda 0A0$ straight leading edge case, assuming that the very near wake quantities in Fig. 18 still retain the hydrodynamics of the upstream turbulent boundary layer. However, for the $\lambda 26A45$ serrated case, in addition to the lift up of turbulent fluids at spanwise location that coincides with the serration troughs ($z/\lambda = \pm 0.5$), Reynolds shear stress $\overline{u'v'}/U_\infty^2$ profiles at spanwise locations that coincide with the serration peaks ($z/\lambda = 0$ and ± 1) do not bear any apparent turbulent boundary layer characteristics for the pressures side. This confirms that the "fingers" of the secondary flows identified earlier in the upstream boundary layer are indeed capable of transporting turbulent fluids away from the wall surface and calming the surrounding flow even beyond the trailing edge, simulatneously. In other words, the entire surface at the pressure side trailing edge no longer retain strong characteristics of a classical turbulent boundary layer.

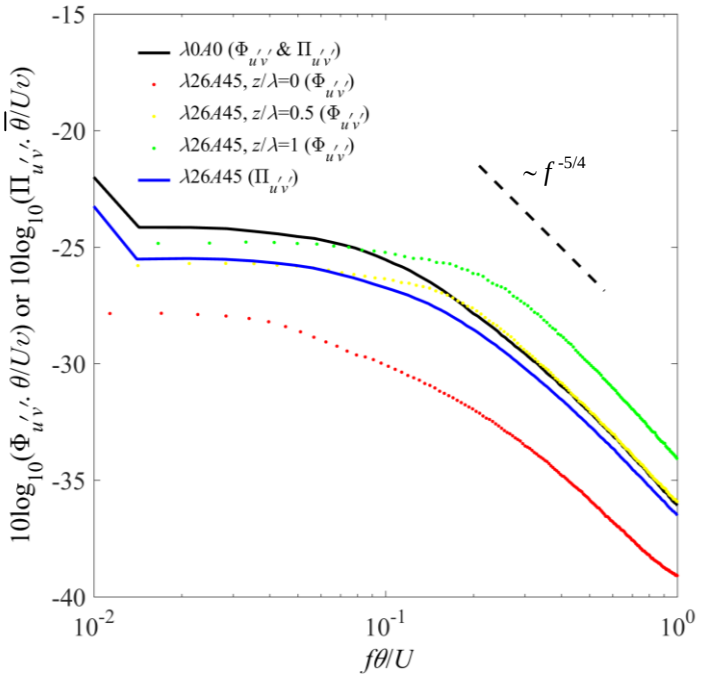

Fig. 19 Comparison of the cross-spectra density: 10 $\log_{10}$ ($\Phi_{u'v'}.\theta/U\nu$), or 10 $\log_{10}$ ($\Pi_{u'v'}.\bar{\theta}/U\nu$), at the very near wake region (x/C = 1.02) produced by aerofoil with the $\lambda 0A0$ baseline and $\lambda 26A45$ serrated leading edges. U = 24 ms^{-1} and the aerofoil is set at 0 degree angle of attack.

Although the Reynolds shear stress $\overline{u'w'}/U_\infty^2$ may not be the most relevant parameter to describe a two-dimensional boundary layer, it is still able to provide some information about the spanwise transport of turbulent flux from the mean flow. Figure 18 also shows the $\overline{u'w'}/U_\infty^2$ contours for the very near wake, which are almost an order of magnitude lower level than the $\overline{u'v'}/U_\infty^2$ counterpart, as produced by both the $\lambda 0A0$ and $\lambda 26A45$ leading edges. Except for the presence of a thin spanwise Reynolds stress component at the suction side of the $\lambda 0A0$ case, which is related to a slight spanwise turbulence transport mechanism in the wake region, the $\overline{u'w'}/U_\infty^2$ is essentially absence at other region in the wake flow. However, prominent $\overline{u'w'}/U_\infty^2$ can be observed at the pressure side of the $\lambda 26A45$ serrated aerofoil. These alternating pairs of prominent Reynolds stress components, which are not demonstrated in the $\lambda 0A0$ aerofoil, indicate that they are of strong secondary flow nature with counter-rotating vortex structures that could sustain beyond the trailing edge.

Having demonstrated the major disruptive nature of the $\lambda 26A45$ serrated leading edge to the turbulent boundary layers on both the suction side and pressure side trailing edge, it is of interest to examine the cross-spectra between the streamwise and normal components of the fluctuating velocity $\phi_{u'v'}$ at the very near wake ($x/C = 1.02$). Instead of selecting several locations in the wake, the analysis focuses on the spatially-integrated cross-spectra density $\Phi_{u'v'}$, as well as the averaged cross-spectra density $\Pi_{u'v'}$. These are defined as below:

$$\Phi_{u'v'}\left(z/\lambda, f\theta/U\right) = \int_{y_1}^{y_2} \phi_{u'v'}\left(y, z/\lambda, f\theta/U\right) dy, \qquad y_1 = -C/5,\ y_2 = C/5 \tag{2.1}$$

$$\Pi_{u'v'}\left(f\theta/U\right) = \frac{1}{N}\sum_{i=1}^{N} \Phi_{u'v'i}\left(z/\lambda, f\theta_i/U_i\right) \tag{2.2}$$

Figure 19 shows the spectra of 10 $\log_{10}$ ($\Phi_{u'v'}.\theta/U\nu$) produced by the $\lambda 0A0$ baseline aerofoil, as well as the $\lambda 26A45$ serrated aerofoil at $z/\lambda = 0$ (peak), 0.5 (mid-region) and 1 (trough). The terms θ, U and ν are used for normalisation of the cross-spectra density, where θ is the momentum thickness of the wake and ν is the kinematic viscosity of air. Similarly, the frequency is non-dimensionalised by (θ/U). For the $\lambda 0A0$ baseline, the cross-spectra density is found to decay at $(f\theta/U)^{-5/4}$ towards the high frequency region, which is slightly lower than the classical -5/3 power law for a turbulent boundary layer. This could be due to the dilution of the integrand in EQ. (2.1) across the upper and lower limits in (y_1, y_2), respectively, which would have included certain portion of the freestream flow. Nevertheless, the same frequency decay of the cross-spectra density is also demonstrated by the $\lambda 26A45$ serrated aerofoil at $z/\lambda = 0$, 0.5 and 1. Interestingly, cross-spectra density at $z/\lambda = 1$ for the serrated aerofoil largely follows the same level at the low frequency end, but begins to deviate at $f\theta/U \geq 0.1$ and surpass the baseline counterpart. For the cross-spectra density at $z/\lambda = 0.5$ of the serrated aerofoil, it largely follows a similar level at $f\theta/U \geq 0.15$, but registers lower level than the baseline case below the frequency. For the serrated case where $z/\lambda = 0$, the corresponding cross-spectra density is significantly lower than the others across the entire frequency range. The different sensitivities of the cross-spectra density across the serration wavelength are averaged and expressed in 10 $\log_{10}$ ($\Pi_{u'v'}.\overline{\theta}/U\nu$), which has been shown to achieve 2–3 dB reduction of the averaged cross-spectra density level over the baseline counterpart at $f\overline{\theta}/U < 0.2$. The level of reduction becomes slightly lower for the serrated aerofoil beyond this frequency. Note that $\overline{\theta}$ is the averaged momentum thickness of the near wake for the $\lambda 26A45$ aerofoil.

The obvious next step is to conduct far field noise measurements for the aerofoil with the $\lambda 0A0$ and $\lambda 26A45$ leading edges, where acoustic spectra for both are compared in Fig. 20. It has been shown earlier that a reduction in the cross-spectra density for the turbulent wake velocities can be achieved at $f\overline{\theta}/U < 0.2$ by the $\lambda 26A45$ serrated aerofoil. Despite showing a significant noise reduction at $0.02 < f\theta/U < 0.6$, it is clear that the reduction is actually related to the turbulence–leading edge interaction noise due to the presence of elevated turbulence in the freestream. At the moment, it is difficult to ascertain whether trailing edge self-noise reduction has indeed been achieved by the leading edge serration at the same frequency range where the turbulence–leading edge noise is so dominant.

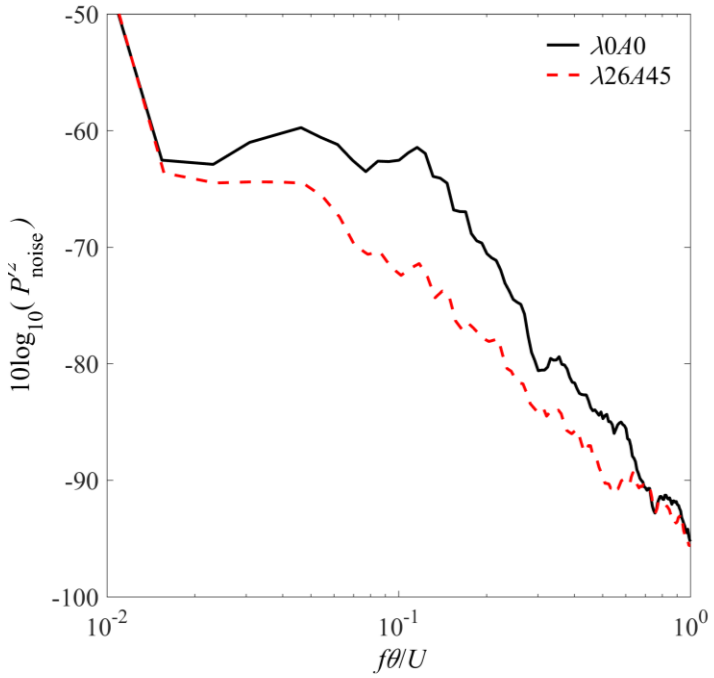

Fig. 20 Comparison of the acoustic spectra produced by aerofoil with the $\lambda 0A0$ baseline and $\lambda 26A45$ serrated leading edges. U = 24 ms^{-1} and the aerofoil is set at 0 degree angle of attack.

VII. Conclusions

This paper presents experimental results on the aeroacoustic performances of a NACA 65(12)-10 aerofoil subjected to serrated leading edges. The serration patterns of these leading edges are formed by cutting into the main body of the aerofoil, instead of extending the leading edges. Therefore these serrated leading edges, when attached to the main body of the aerofoil, will always result in the same overall chord length. The experiment was performed in an aeroacoustic wind tunnel facility. These serrated leading edges were investigated for their effectiveness in suppressing four different types of noise sources: laminar instability tonal noise, leading edge separation bubble noise, turbulence–leading edge interaction noise and trailing edge self-noise. Below are the main outcomes from the investigation:

1. Streamwise vortices produced by an optimised serrated leading edge can suppress the separation bubble at the trailing edge, thereby reducing the instability laminar tonal noise significantly. It is found that the most effective serration configuration is the one with the largest serration amplitude and smallest serration wavelength.
2. Without even relying on the streamwise vortices, the sawtooth geometry of the serration itself can already be sufficient to suppress the leading edge separation bubble. Due to the special geometry of the NACA 65(12)-10, it is very effective in the production of laminar separation bubble noise at the leading edge. The use of serrated leading edge can therefore be an effective passive device to suppress this particular noise source.
3. Similar to point 1 above, the most effective serration geometry in the reduction of turbulence–leading edge interaction noise is the one with the largest serration amplitude and smallest serration wavelength. However, this configuration is also prone to generating superfluous noise at high frequency.
4. Extensive boundary layer and very near wake measurements were performed to investigate the flow structures on the NACA 65(12)-10 aerofoil with a large serration amplitude leading edge. It can be concluded that the serrated leading edge is very disruptive to the hydrodynamic growth of the turbulent boundary layer at the trailing edge. Evidences on the reduction of boundary layer low-frequency turbulence at the trailing edge could support the hypothesis of a reduction in the low-frequency far field noise. This remains to be confirmed in the future studies.

Acknowledgment

This project is supported by the EPSRC on Research Grant No: EP/N018737/1 “Quiet Aerofoils of the Next-Generation”.

References

[1] Chong TP, Dubois E, Optimization of the poro-serrated trailing edges for broadband noise reduction, Journal of the Acoustical Society of America 140 (2016) 11361–1373.
[2] Vathylakis A, Chong TP, Joseph PF, Poro-serrated trailing-edge devices for airfoil self-noise reduction, AIAA Journal 53 (2015) 3379–3394.
[3] Chong TP, Vathylakis A, Joseph PF, Gruber M, Self-noise produced by an airfoil with nonflat plate trailing-edge serrations, AIAA Journal 51 (2013) 2665-2677.
[4] Gruber M, Joseph PF, Chong TP, On the mechanisms of serrated airfoil trailing edge noise reduction, 17th AIAA/CEAS Aeroacoustic Conference, AIAA-2011–2781, Portland, USA, 2011
[5] Oerlemans S, Fisher M, Maeder T, Korler K, Reduction of wind turbine noise using optimized airfoils and trailing edge serrations, AIAA Journal 47 (2009) 1470–1481.
[6] Hurault J, Gupta A, Sloth E, Nielsen NC, Borgoltz A, Ravetta P, Aeroacoustic wind tunnel experiment for serration design optimisation and its application to a wind turbine rotor, 6th International Meeting on Wind Turbine Noise, Glasgow, UK, 2015
[7] Gruber M, Joseph PF, Polacsek C, Chong TP, Noise reduction using combined trailing edge and leading edge serrations in a tandem airfoil experiment, 18th AIAA/CEAS Aeroacoustic Conference, AIAA-2012–2134, Colorado Springs, USA, 2012
[8] Narayanan S, Joseph PF, Haeri S, Kim JW, Chaitanya P, Polacsek C. Noise reduction studies from the leading edge of serrated flat plates, 20th AIAA/CEAS Aeroacoustic Conference, AIAA-2014-2320, Atlanta, USA, 2014.
[9] Biedermann TM, Chong TP, Kameier F, Paschereit CO, Statistical-empirical modelling of airfoil noise subjected to leading edge serrations, AIAA Journal 55 (2017) 3128–3142.
[10] Kim JW, Haeri S, Joseph PF, On the reduction of aerofoil-turbulence interaction noise associated with wavy leading edges, Journal of Fluid Mechanics 792 (2016) 526-552.
[11] Turner J, Kim JW, Towards understanding aerofoils with wavy leading edges interacting with vortical disturbances, 22nd AIAA/CEAS Aeroacoustics Conference, AIAA-2016-2952, Lyon, France, 2016.
[12] Lacagnina G, Hasheminejad SM, Chaitanya P, Joseph PF, Chong TP, Stalnov O, Leading edge serrations for the reduction of aerofoil separation self-noise, 24th AIAA/CEAS Aeroacoustics Conference, AIAA-2017-4169, Denver, USA, 2017.
[13] Vathylakis A, Kim JH, Chong TP, Design of a low-noise aeroacosutic wind tunnel facility at Brunel University. 20th AIAA/CEAS Aeroacoustic Conference, AIAA-2014-3288, Atlanta, USA, 2014
[14] Laws EM, Livesey JL, Flow through screens, Annual Review of Fluid Mechanics 10 (1978) 247-266.
[15] Rozenberg Y, Modélisation analytique du bruit aérodynamique à large bande des machines tournantes : utilisation de calculs moyennés de méanique des fluids, Acoustics. Ecole Centrale de Lyon, Lyon, France, 2007.
[16] Paterson R, Vogt P, Fink M, Munch C, Vortex noise of isolated airfoils, Journal of Aircraft 10 (1973) 296-302.
[17] Arbey H, Bataille J, Noise generated by airfoil profiles placed in a uniform laminar flow, Journal of Fluids Mechanics 134 (1983) 33-47.
[18] Chong TP, Joseph PF, Kingan MJ, An investigation of airfoil tonal noise at different Reynolds numbers and angles of attack, Applied Acoustics 74 (2013) 38-48.
[19] Chaitanya P, Aerofoil geometry effects on turbulence interaction noise, PhD thesis, University of Southampton, UK, 2017.